Search for New Forms of Hadronic Matter in Photoproduction

P. Eugenio (FSU)*†, C. Salgado ($NSU/JLab$)*, D. P. Weygand ($JLab$)*,
A. Afanasev ($JLab$), V. D. Burkert ($JLab$), S. Capstick (FSU),
P. L. Cole ($JLab$), P. Coltharp (FSU), D. Ireland ($Glasgow$),
L. Guo ($JLab$), J. Kellie ($Glasgow$), M. Khandaker ($NSU/JLab$),
K. Livingston ($Glasgow$), C. A. Meyer (CMU), M. Nozar ($JLab$),
A. Ostrovidov (FSU), E. S. Smith ($JLab$), B. Stokes (FSU),
M. Wood (USC),
and the CLAS Collaboration

December 2, 2003

Abstract

We propose to search for new forms of hadronic matter utilizing a photon beam at CLAS in Hall B. Motivated by recent experimental results for gluonic hybrid meson candidates and from recent theoretical Lattice QCD and Flux-tube model calculations, photoproduction should provide an ideal hunting ground for gluonic matter. Jefferson Lab offers an excellent opportunity to undertake the study of meson spectroscopy at intermediate energies. Current studies are underway at CLAS which show the feasibility of using CLAS as a meson spectrometer for few-body final states. We propose to perform meson spectroscopy using CLAS, in Hall B. We will study reactions having multiple charged particles in the final state, of the form $\gamma p \rightarrow$: $p\pi^+\pi^-\pi^\circ$, $n\pi^+\pi^+\pi^-$, $pK^+K^-\eta$, $nK^+K^+\pi^-$, $\Delta^{++}\eta\pi^-$, $pp\bar{p}$.

1 Motivations

Discoveries of new phenomena in nuclear and particle physics have provided insight into the fundamental constituents of matter. In the past few decades we have seen a new picture emerge in which quarks form the building blocks of nearly all matter. Yet

*Spokesperson
†Contactperson

the gluon, which carries the force which binds quarks, can interact with other gluons to form a bound state, or interact as a fundamental constituent of matter along with the quarks. Thus new forms of gluonic or hybrid matter should exist.

The search for hybrids in recent years has resulted in considerable excitement. Theoretical predictions from both gluonic flux-tube models and recent lattice gauge theory results predict the lightest hybrid at a mass of 1.9 GeV for the exotic $J^{PC} = 1^{-+}$ $q\bar{q}g$-hybrid(see references [1] and [2]). Exotic meson states are those with quantum numbers not accessible to conventional $q\bar{q}$ bound states. Recent experimental results find two very promising 1^{-+} exotic candidates. The $\pi_1(1400)$ seen decaying to $\eta\pi^-$ at Brookhaven has a mass somewhat too low for the theory prediction for a gluonic hybrid [3]. A higher mass observed state, the $\pi_1(1600)$ is tantalizing as a gluonic hybrid, but its decay to $\rho\pi$ was unexpected [4]. Even though the existence of both states appears very clear, these states have had a history of controversy, particular those produced via pion beams [5].

It has been pointed out by Close and Page [6] that in the case of photoproduction, where the photon can be effectively replaced by a ρ interacting with an exchange π, ρ, or ω, the production strength for producing gluonic hybrids could be considerable. Furthermore, Szczepaniak and Swat [7] concluded that in the case of photoproduction, the π_1 exotic and the well known a_2 should be produced on an equal footing, whereas in pion production the exotic is suppressed by a factor of 10.

As supported by recent lattice gauge calculations using excited adiabatic potentials, it is a good approximation to decouple the quark degrees of freedom from the gluonic degrees of freedom. This is based on the idea that quarks in the systems react much slower than the gluonic fields responsible for strong confinement. As in ordinary $q\bar{q}$ mesons where the addition of one unit of orbital angular momentum costs about 1 GeV, calculations show that gluonic excitations are also of the order of 1 GeV in energy, and that there is a kind of orthogonality decoupling the quarks and flux-tube (gluon) degrees of freedom. In lattice QCD calculations and in flux-tube models, excited flux-tubes can have

$$_{flux-tube}J^{PC} = 1^{+-} \text{ or } 1^{-+} \text{ [8].}$$

Therefore with pseudoscalar probes, such as pion beams, coupling the quark degrees of freedom to those of an excited flux-tube results in

$$_{quarks}J^{PC} \otimes_{flux-tube} J^{PC} = 1^{--}, 1^{++}.$$

On the other hand, for vector probes, such as the photon viewed as a vector meson, coupling the quark degrees of freedom with that of an excited flux-tube results in

$$_{quarks}J^{PC} \otimes_{flux-tube} J^{PC} = 0^{-+}, 1^{-+}, 2^{-+}, 0^{+-}, 1^{+-}, 2^{+-}.$$

It is interesting to note that the vector probe has access to manifestly exotic quantum numbers (exotic $J^{PC} = 0^{+-}, 1^{-+}, 2^{+-}$). Since there exists a wealth of data with

Table 1: A sample of measured photoproduction cross sections. Note the small yields in all channels.

Reaction	E_γ[GeV]	Events
$\gamma p \to p\pi^+\pi^-$	9.3	3500
$\gamma p \to p\pi^+\pi^-$	19.3	20980
$\gamma p \to p\pi^+\pi^-\pi^\circ$	4.7	1606
$\gamma p \to p\pi^+\pi^-\pi^\circ$	9.3	1195
$\gamma p \to p\pi^+\pi^-\pi^\circ$	4.7-5.8	3001
$\gamma p \to p\pi^+\pi^-\pi^\circ$	6.8-8.2	7297
$\gamma p \to p\pi^+\pi^-\pi^\circ$	20-70	14236
$\gamma p \to n\pi^+\pi^+\pi^-$	4.7-5.8	1723
$\gamma p \to n\pi^+\pi^+\pi^-$	6.8-8.2	4401
$\gamma p \to n\pi^+\pi^+\pi^-$	16.5-20	3781
$\gamma p \to p\pi^+\pi^-\pi^+\pi^-$	4.0-6.0	~ 300
$\gamma p \to p\pi^+\pi^-\pi^+\pi^-$	6.0-8.0	~ 500
$\gamma p \to p\pi^+\pi^-\pi^+\pi^-$	8.0-12.0	~ 500
$\gamma p \to p\pi^+\pi^-\pi^+\pi^-$	12.0-18.0	~ 400
$\gamma p \to p\pi^+\pi^-\pi^+\pi^-$	15.0-20.0	~ 400
$\gamma p \to p\pi^+\pi^-\pi^\circ\pi^\circ$	20-70	8100
$\gamma p \to p\pi^+\pi^-\pi^+\pi^-\pi^\circ\pi^\circ$	19.5	2553
$\gamma p \to \Delta^{++}\pi^+\pi^-\pi^-$	4.0-6.0	~ 200
$\gamma p \to \Delta^{++}\pi^+\pi^-\pi^-$	6.0-8.0	~ 200
$\gamma p \to \Delta^{++}\pi^+\pi^-\pi^-$	8.0-12.0	~ 200
$\gamma p \to \Delta^{++}\pi^+\pi^-\pi^-$	12.0-18.0	~ 200

pseudoscalar hadronic probes and very little data with vector probes like the photon, this may explain the lack of observations of gluonic hybrids. Table 1 provides a list of photoproduction yields from previous experiments [9][1]. It is clear that these yields are extremely small, and that determination of a state's J^{PC} through partial wave analysis requires substantial yields, even for a dominant signal. Such an analysis is required in order to definitively discover an exotic.

Flux-tube model calculations of gluonic hybrid decays prefer decay channels to (L=0) + (L=1) meson pairs. For example, according to these calculations the lowest lying exotic state ($J^{PC} = 1^{-+}$) should have typical partial widths [10]

$$b_1\pi : f_1\pi : \rho\pi = 170\ MeV : 60\ MeV : 10\ MeV.$$

Figure 1 shows the $b_1\pi$ invariant mass for a recent analysis of SLAC photoproduction data [11]. The sparse data clearly demonstrates the need for better photoproduction experiments.

[1]Results from CLAS will be presented in a later section

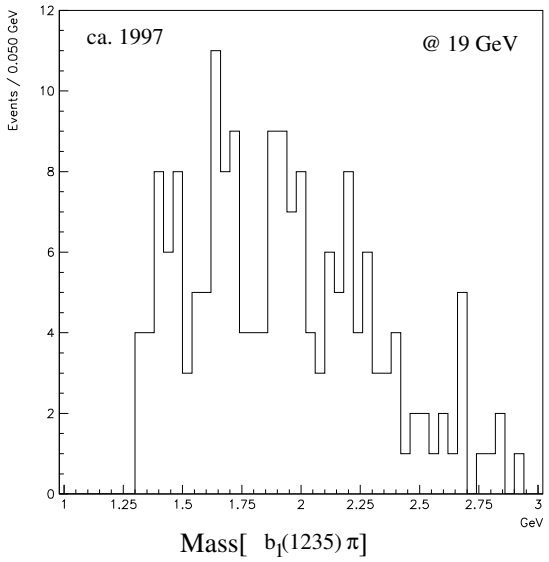

Figure 1: The $b_1(1235)\pi$ mass spectrum from $\gamma p \to p\pi^+\pi^+\pi^-\pi^-\pi^0$ at 16.5 -21.0 GeV.

Studies are underway to pursue gluonic matter at nuclear physics labs around the world. At JLab there are plans to upgrade the accelerator by doubling its maximum beam energy. A linchpin for the Lab's upgrade plans[2] is the addition of a new experimental program called GlueX[3]. The goal of GlueX is to unambiguously discover and study gluonic matter. Although GlueX will be the definitive experiment for studying gluonic matter, it will be several years until this experimental program begins to acquire data. In the meantime, we are proposing a timely and complementary experimental program in meson spectroscopy which will search for new and unusual mesons via photoproduction using the CLAS detection facility at Jefferson Lab.

The promising results from BNL-E852 have provided strong candidates for exotic mesons whose identity may correspond to either gluonic hybrids or four-quark composites. An important logical step in a study of exotic mesons is to look for those containing $s\bar{s}$, that is strangeonium hybrids, and exotic strangeonia. Photoproduction is an excellent technique for producing $s\bar{s}$ mesons due to the vector nature of the beam. According to the vector meson dominance model, one expects the interactions to occur via the vector mesons $\rho^0 : \omega : \phi$ with relative strengths $9 : 1 : 2$ respectively. This provides a natural way to embed $s\bar{s}$ directly into the system.

Also important is exploration of the ordinary strangeonia. These are mesons made of dominantly $s\bar{s}$ unflavored strange quarkonia which are associated with the radial and orbital excited states of the $\phi(1020)$ meson– the ground state of the vector $s\bar{s}$ system. Strangeonia are poorly understood – of the 22 strangeonium states

			J^{PC}	**Name**	**Mass (MeV)**
n=2	L=0	S=0	0^{-+}	η_s	1415
		S=1	1^{--}	ϕ	1680
	L=1	S=0	1^{+-}	h_1	1850
		S=1	0^{++}	f_0	2000
			1^{++}	f_1	1950
			2^{++}	f_2	2000
n=3	L=0	S=0	0^{-+}	η_s	1950
		S=1	1^{--}	ϕ	2050

Table 2: Radial Excitations of (I=0,$s\bar{s}$) Mesons

			J^{PC}	**Name**	**Mass (MeV)**
n=1	L=0	S=0	0^{-+}	η,$\eta^{'}$	548,958
		S=1	1^{--}	ϕ	1020
	L=1	S=0	1^{+-}	$h_1^{'}$	1380
		S=1	0^{++}	$f_0^{'}$	1500
			1^{++}	$f_1^{'}$	1530
			2^{++}	$f_2^{'}$	1525
	L=2	S=0	2^{-+}	$\eta_2^{'}$	1850
		S=1	1^{--}	ϕ_1	1850
			2^{--}	ϕ_2	1850
			3^{--}	ϕ_3	1854

Table 3: Orbital Excitations of (I=0,$s\bar{s}$) Mesons

expected below a mass of 2.2 GeV, only 5 are well identified. The clarification of the strangeonium spectra in this mass range is an important and necessary step for the advancement of meson spectroscopy. Given that strangeonium states have intermediate masses between the light (up, down) and heavy (charm, bottom) quarkonia, they are very useful in the study of the QCD confinement potential in the transition region from short to large distance behavior. Particularly, $s\bar{s}$ excitations provide a range of quark separations where the confinement potential can be explored from the perturbative to the non-perturbative regimes. This character has been pointed out by Gell-Mann and recently by Barnes, Page and Black [13]: "the similarity between the $s\bar{s}$ spectrum, the light meson $n\bar{n}$ and the heavy $Q\bar{Q}$ systems needs to be understood to bridge the gap between Heavy Quark Effective Theory (HQET) and the light quark world in which we live".

Table 2 and 3 summarized the predicted orbital and radial excited states of (I=0,$s\bar{s}$) conventional mesons. Table 4 shows a list of the low-lying hybrid exotic

Exotic $s\bar{s}g$ States	Decay Mode	Partial Width
2^{+-} $h_2{}'(2100)$	$\rightarrow K_2^*(1430)K$	90 MeV
	$\rightarrow K_1(1270)K$	30 MeV
	$\rightarrow K_1(1400)K$	70 MeV
1^{-+} $\eta_1{}'(2100)$	$\rightarrow K_1(1270)K$	100 MeV
	$\rightarrow K_1(1400)K$	250 MeV
0^{+-} $h_0{}'(2100)$	$\rightarrow K_1(1270)K$	400 MeV
	$\rightarrow K_1(1400)K$	175 MeV

Table 4: Low-lying exotic strangeonia states predicted by the flux model[6] with a $s\bar{s}$ component

states predicted by the flux model with a $s\bar{s}$ component. Predictions for masses and widths of all these excitations are available within the flux tube model [13]. Decays have been calculated in the $^3P_0$. However, production mechanisms are not fully understood.

Due to the high $s\bar{s}$ content of the photon, and the high luminosity beams available, photoproduction of mesons with significant $s\bar{s}$ content are expected to take place with unprecedented statistics at Jefferson Lab. The proposed study, using 5-6 GeV photons, will also probe $\phi(1680)$ and $\phi(1850)$ production. The $\phi(1680)$, a $2S(J^{PC} = 1^{--})$ radial excitation, has been seen in electro-production [14] and photoproduction [15].

A summary of the current data on the $\phi(1680)$ is shown in Table 5. The interpretation of the current data is not conclusive. Photoproduction and electroproduction experiments have observed different properties of the $\phi(1680)$ decay modes. The mass of the resonance is consistently higher in photoproduction than in e^+e^- production. Furthermore, there is no evidence of KK^* decay in photoproduction, however, in e^+e^- this channel is dominant. Barnes, Page and Black predict the relative decays strengths of the $\phi(1680)$ meson to KK, KK^*, and $\phi\eta$ to be $2:5:1$, respectively [13].

The different behavior of the $\phi(1680)$ observations in photo- and electroproduction may be possible by the presence of two states interfering with $n\bar{n}$ states. To understand this problem one will need to measure relative branching ratios of the $\phi(1680)$ into the neutral and charged KK and KK^* modes. However, the cleanest decay mode to study should be the $\phi\eta$ channel, where interference with $n\bar{n}$ states is highly suppressed. According to the Zweig rule, the $\phi\eta$ channel can arise *only* from $s\bar{s}$ initial states. This decay mode has not been yet observed, and its study is one of the goals of this proposal. Just the mere identification (or not identification) of a resonance in the $\phi\eta$ system will signal the presence of a $s\bar{s}$ state.

It is generally accepted that diffraction [27] is the dominant mechanism for the photoproduction of vector meson resonances. This is certainly true at high energies, from example at HERA and Fermilab energies where the data are compatible with Pomeron exchange. However, at intermediate energies (where JLab probes), the

production	mass(MeV)	width(MeV)	*experiment*	decay	ref
e^+e^-	1650		DM1	K_LK_S	[18]
	1650			K^+K^-	[19]
	1650		VEPP-2M	K^+K^-	[20]
	1680		DM2	K^+K^-	[21]
	1677	102		$K_SK^+\pi^-$.	[16]
	1680	185	DM1	KK, $KK\pi$	[22]
	1657	146	DM2	K^+K^-	[23]
photo-	1748	80	CERN Omega	KK	[24]
	1760	80	CERN WA57	KK	[25]
	1726	121	Fermi E401	KK	[26]
	1753	122	Fermi FOCUS	KK	[17]

Table 5: Experimental data on the $\phi(1680)$

theoretical answer is not so clear because other mechanisms should be considered. For example, a likely mechanism is π exchange since the π couples strongly to the ρ, and so there can be both strong pseudo-vector and tensor production.

2 Partial Wave Analysis

Intensity Distributions

The differential cross-section for a photoproduction reaction determines the intensity distribution, I(τ), and therefore the number of events as a function of total mass and t. This intensity distribution is one of the major observables that a partial wave analysis(PWA) attempts to match. It is necessary to perform a PWA to clearly identify the J^{PC} quantum numbers of a meson resonance. A partial wave analysis fits the measured observables such as angular and kinematic distributions to determine the production strength of each partial wave. For a photon beam, the intensity distribution can be written as[30]

$$I(\tau) = \sum_{k\epsilon\epsilon'} \epsilon\epsilon' \rho_{\epsilon\epsilon'}(\tau) \sum_{\alpha\alpha'} {}^{k\epsilon'}V^*_{\alpha'} \ {}^{\epsilon'}A^*_{\alpha'}(\tau) \ {}^{k\epsilon}V_{\alpha} \ {}^{\epsilon}A^*_{\alpha}(\tau)$$

The intensity distribution is characterized by a set of interfering (denoted by α and ϵ) and non-interfering (denoted by k) orthonormal amplitudes. The variable τ represents collectively all the variables necessary to have a complete description of the final state. Often τ includes the produced and intermediate meson masses, decay angles, and four-momentum transfer t. The superscript k represents the initial and final spin orientations in the production process. The above amplitudes are expressed

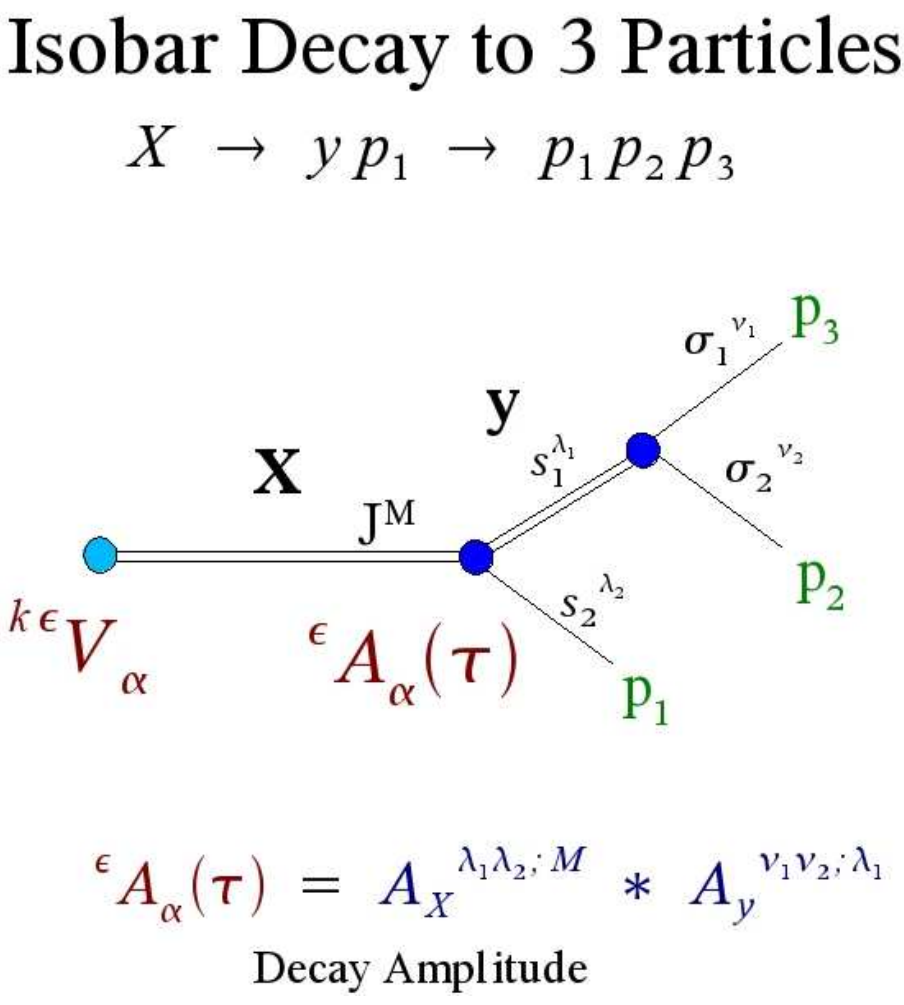

Figure 2: Isobar decay to three final state particles. The calculation of the decay amplitudes ${}^{\epsilon}A_\alpha(\tau)$ is based primarily on conservation of angular momentum and parity, with limited phenomenological input from the Isobar Model. The production amplitudes ${}^{k\epsilon}V_\alpha$ are the complex production strengths. The production amplitudes are the unknown complex parameters which are varied during a partial wave analysis fit to best describe the observed intensity distribution.

in the reflectivity basis (denoted by ϵ), which takes into account parity conservation in the production process by a transformation of helicity states to eigenstates of the reflection operator in the production plane. The photon spin-density matrix in the reflectivity basis is

$$\rho_{\epsilon\epsilon'}(\tau) = \begin{pmatrix} \frac{1}{2}(1 - P[cos^2(\delta) - sin^2(\delta)]) & Pcos(\delta)sin(\delta) \\ Pcos(\delta)sin(\delta) & \frac{1}{2}(1 + P[cos^2(\delta) - sin^2(\delta)]) \end{pmatrix}$$

Note that states with different reflectivity, ϵ, only interfere through the off-diagonal elements of the photon spin-density matrix. For unpolarized photons ($P = 0$), states with different reflectivity do not interfere at all.

Following the prescription of the isobar model, the total amplitude is factorized into a production amplitude ${}^{k\epsilon}V_\alpha$, and a decay amplitude ${}^{\epsilon}A_\alpha(\tau)$. The calculation of the decay amplitudes ${}^{\epsilon}A_\alpha(\tau)$ is based primarily on conservation of angular momentum and parity, with limited phenomenological input from the Isobar Model. In the reflectivity basis, the decay amplitudes are given by [12]

$${}^{\epsilon}A_\alpha(\tau) = \Theta(M)\{A_\alpha^{JM}(\tau) - \epsilon P_X(-1)^{P_X - M} A_\alpha^{J-M}(\tau)\}$$

where $\Theta(M) = \frac{1}{\sqrt{2}}, \frac{1}{2}, 0$ for $M > 0, M = 0$, and $M < 0$ respectively. P_X is the parity of the meson system, and J, M are the usual total meson angular momentum and its projection. The total helicity decay amplitude is a product of decay amplitudes for each sequential decay in the decay chain ($A_\alpha^{JM}(\tau) = A_X^{\lambda_1\lambda_2;M} * A_y^{\nu_1\nu_2;\lambda_1} * ...$) where $\lambda = \lambda_1 - \lambda_2$ is the total two-body CM helicity(See Figure 2. At each vertex the decay amplitude is given in terms of a Wigner D-function, Clebsch-Gordan Coefficients, and a mass dependent factor K which is often of a Breit-Wigner or K-Matrix form

$$A_X^{\lambda_1\lambda_2;M} = D^J_{\lambda M}(\theta, \phi)\frac{\sqrt{L(L+1)}}{\sqrt{J(J+1)}}(L0; S\lambda|J\lambda)(S_1\lambda_1; S_2 - \lambda_2; |S\lambda)K$$

The production amplitudes ${}^{k\epsilon}V_\alpha$ are the complex production strengths. These are the unknown complex parameters which are varied during a partial wave analysis fit to best describe the observed intensity distribution.

Extended Maximum Likelihood Fit

An extended maximum likelihood fit is used to determine the production amplitudes that best describe the data. The program that performs the fit uses the CERNLIB routine Minuit to maximize the log of the likelihood[31].

The likelihood function for finding N_o observed events in a given bin is

$$\mathcal{L} = e^{-\overline{N_o}({}^{\epsilon}V_{k\alpha})} \prod_i^{N_o} F({}^{\epsilon}V_{k\alpha}; \tau_i),$$

where

$$F({}^{\epsilon}V_{k\alpha};\tau_i) = I(\tau_i) = \sum_{k,\epsilon,\alpha,\alpha'} {}^{\epsilon}V_{k\alpha}\,{}^{\epsilon}V^*_{k\alpha'}\,{}^{\epsilon}A_{\alpha}(\tau_i)\,{}^{\epsilon}A^*_{\alpha'}(\tau_i)$$

is the intensity distribution and

$$\overline{N_o}({}^{\epsilon}V_{k\alpha}) = \int I(\tau)\eta(\tau)pq\,d\tau = \sum_{k,\epsilon,\alpha,\alpha'} {}^{\epsilon}V_{k\alpha}\,{}^{\epsilon}V^*_{k\alpha'} \int {}^{\epsilon}A_{\alpha}(\tau)\,{}^{\epsilon}A^*_{\alpha'}(\tau)\eta(\tau)pq\,d\tau$$

is the average number of events one would observe if the same experiment were repeated many times[32]. The experimental acceptance is represented by $\eta(\tau)$, and $pq\,d\tau$ represent the Lorentz-invariant phase-space element.

The integrals over the decay amplitudes are often called the accepted normalization integrals[33],

$${}^{\epsilon}\Phi^{\eta}_{\alpha\alpha'} = \int {}^{\epsilon}A_{\alpha}(\tau)\,{}^{\epsilon}A^*_{\alpha'}(\tau)\eta(\tau)pq\,d\tau.$$

Since the acceptance $\eta(\tau)$ is not known analytically, the accepted normalization integrals are evaluated using Monte Carlo events where the effects of the experiment are modeled to account for the experimental acceptance

$${}^{\epsilon}\Phi^{\eta}_{\alpha\alpha'} = \frac{1}{N_r}\sum_{i}^{N_\eta} {}^{\epsilon}A_{\alpha}(\tau_i)\,{}^{\epsilon}A^*_{\alpha'}(\tau_i).$$

The sum is over the accepted Monte Carlo data, where N_r is the number of raw Monte Carlo events generated to end up with a set of N_η accepted events. The phase-space factor is taken into account by generating the Monte Carlo events according to a phase-space distribution.

The extended log-likelihood function which is maximized now becomes

$$\ln\mathcal{L} = \sum_{i}^{N_o} \ln(F({}^{\epsilon}V_{k\alpha};\tau_i)) - \overline{N_o}({}^{\epsilon}V_{k\alpha})$$

$$\ln\mathcal{L} = \sum_{i}^{N_o} \ln\{\sum_{k,\epsilon,\alpha,\alpha'} {}^{\epsilon}V_{k\alpha}\,{}^{\epsilon}V^*_{k\alpha'}\,{}^{\epsilon}A_{\alpha}(\tau)\,{}^{\epsilon}A^*_{\alpha'}(\tau)\} - \sum_{k,\epsilon,\alpha,\alpha'} {}^{\epsilon}V_{k\alpha}\,{}^{\epsilon}V^*_{k\alpha'}\,{}^{\epsilon}\Phi^{\eta}_{\alpha\alpha'}.$$

The average number of events corrected for acceptance (N_c) can be calculated using the set of N_r raw Monte Carlo events along with the fitted results for the production amplitudes by the following relation

$$\overline{N_c}({}^{\epsilon}V_{k\alpha}) = \int I(\tau)pq\,d\tau = \sum_{k,\epsilon,\alpha,\alpha'} {}^{\epsilon}V_{k\alpha}\,{}^{\epsilon}V^*_{k\alpha'}\,{}^{\epsilon}\Phi_{\alpha\alpha'},$$

where

$${}^{\epsilon}\Phi_{\alpha\alpha'} = \frac{1}{N_r}\sum_{i}^{N_r} {}^{\epsilon}A_{\alpha}(\tau)\,{}^{\epsilon}A^*_{\alpha'}(\tau)$$

are the raw normalization integrals. They are calculated just like the accepted normalization integrals except that the Monte Carlo events are not subjected to a simulation of the experimental apparatus.

In practice, the production amplitudes are renormalized via

$$V \rightarrow \sqrt{N_o \frac{N_r}{N_\eta}} V.$$

Neglecting the constant log term, the log-likelihood function becomes

$$ln\mathcal{L} = \sum_i^{N_o} ln(\sum_{k,\epsilon,\alpha,\alpha'} {}^{\epsilon}V_{k\alpha}\, {}^{\epsilon}V^*_{k\alpha'}\, {}^{\epsilon}A_\alpha(\tau)\, {}^{\epsilon}A^*_{\alpha'}(\tau)) - N_o \frac{N_r}{N_\eta} \sum_{k,\epsilon,\alpha,\alpha'} {}^{\epsilon}V_{k\alpha}\, {}^{\epsilon}V^*_{k\alpha'}\, {}^{\epsilon}\Phi^\eta_{\alpha\alpha'}.$$

It is advantageous to renormalize because, to first order, the renormalized production amplitudes are independent of variations in the number of events among different bins, and therefore they are excellent starting values for neighboring bins[33].

Calculation of Observables

The acceptance-corrected number of events is after renormalization,

$$\overline{N_c}({}^{\epsilon}V_{k\alpha}) = N_o \frac{N_r}{N_\eta} \sum_{k,\epsilon,\alpha,\alpha'} {}^{\epsilon}V_{k\alpha}\, {}^{\epsilon}V^*_{k\alpha'}\, {}^{\epsilon}\Phi_{\alpha\alpha'}.$$

The acceptance corrected number of events attributed to a state $|\alpha, \epsilon\rangle$ is

$$\overline{N_{|\alpha,\epsilon\rangle}} = N_o \frac{N_r}{N_\eta} \sum_k |\, {}^{\epsilon}V_{k\alpha}|^2\, {}^{\epsilon}\Phi_{\alpha\alpha},$$

and the phase difference between two states $|\alpha, \epsilon\rangle$ and $|\alpha', \epsilon\rangle$ is

$$\phi_{\alpha\alpha'\epsilon} = \arg(\sum_k {}^{\epsilon}V_{k\alpha}\, {}^{\epsilon}V^*_{k\alpha'}).$$

The above phase is only meaningful if states $|\alpha, \epsilon, k\rangle$ and $|\alpha, \epsilon, k'\rangle$ are produced coherently. A measure of the coherence is given by

$${}^{\epsilon}C_{\alpha\alpha'} = \frac{|\sum_k {}^{\epsilon}V_{k\alpha}\, {}^{\epsilon}V^*_{k\alpha'}|}{\sqrt{(\sum_k |{}^{\epsilon}V_{k\alpha}|^2)(\sum_k |{}^{\epsilon}V_{k\alpha'}|^2)}}.$$

3 PWA Study of Simulated Data

To help in understanding the limits of the CLAS acceptance and to help in the development of the PWA tools, a partial wave analysis study was performed on Monte Carlo events to simulate meson production via photoproduction. Events of the form

$\gamma p \to pX \to p\rho\pi \to p\pi^+\pi^+\pi^-$ were generated according to t-channel phase space with a $\partial\sigma/\partial t \propto e^{5t}$. These events were then weighted according to a photoproduction cross-section for unpolarized 5 GeV/c^2 photons, and with a one pion exchange production OPE mechanism[34]. Included in the description of the cross-section were 4 resonances: $a_1(1260)$, $a_2(1320)$, $\pi_1(1600)$, and $\pi_2(1670)$.

These events were put through a simulation of the CLAS detector using the GEANT-based standard CLAS simulation program GSIM. The resulting simulated data were then processed using the standard CLAS event reconstruction program (a1c) that is used to reconstruct experimental acquired CLAS data. Final event selection required standard cuts, including the identification of $\pi^-2\pi^+$ in CLAS and the recoil neutron identification via missing mass. Figure 3 shows the accepted $\pi^+\pi^+\pi^-$ invariant mass for the simulated events(a total of 170,000). The two main features are the $a_1(1260)/a_2(1320)$ region near 1.3 GeV/c^2 and the $\pi_2(1670)/\pi_1(1600)$ region near 1.6 GeV/c^2.

A mass independent partial wave analysis of the simulated data was performed using 20 MeV/c^2 wide mass bins from 1.0 GeV/c^2 to 2.0 GeV/c^2. Eighteen partial waves were used in the PWA fit. For each of $J^{PC}|M|^\epsilon L$ there were two waves corresponding to both positive and negative reflectivity: $2^{++}1^\epsilon D$, $1^{++}1^\epsilon S$, $2^{-+}1^\epsilon$, $1^{-+}1^\epsilon P$, $1^{++}1^\epsilon D$, $2^{-+}1^\epsilon F$, $2^{++}2^\epsilon D$, $2^{-+}2^\epsilon P$, and $3^{++}1^\epsilon F$. In this notation, $J^{PC}|M|^\epsilon L$ refer to the total 3π system's: spin, parity, C-parity, absolute value of spin projection on the axis of quantization, reflectivity, and the relative orbital angular momentum between the ρ and π. A separate PWA fit is performed in each mass bin independent of neighboring mass bins. The PWA intensities resulting from the many mass independent PWA fits are shown in Figures 4 and 5. Shown are results for positive reflectivity. Negative reflectivity results are nearly identical. For unpolarized photon beams, the PWA fit cannot distinguish between positive and negative reflectivities and splits the strengths equally. This is due to the fact that an unpolarized (or circularly polarized) photon beam is not an eigenstate of parity. The results shown in Figure 4 demonstrate the ability of the PWA to extract the different resonances in their proper partial waves. The $a_1(1260)$, $a_2(1320)$, $\pi_2(1670)$, and $\pi_1(1600)$ are exhibited in $1^{++}1^+$, $2^{++}1^+$, $2^{-+}1^+$, and $1^{-+}1^+$ partial waves, respectively. Partial waves for which one does not expect to observe resonance structure are show in Figure 5. The maximum yield is more than an order of magnitude smaller, and the resulting intensities are consistent with zero.

4 Recent Results from CLAS Photoproduction at High Energies

The CLAS collaboration took data at the end of August 2001 with a real photon beam with an energy range of 4.8 GeV to 5.47 GeV. Since the CLAS detector is not well designed to study forward-going systems, this effort used a modified orientation of the

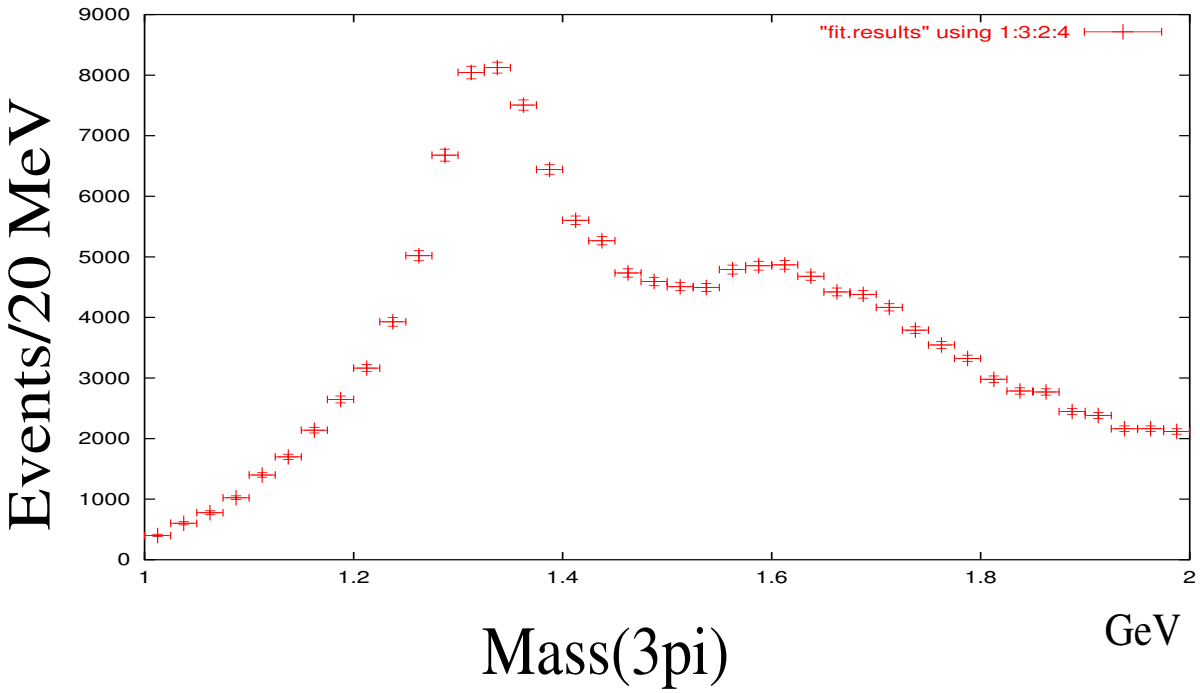

Figure 3: The accepted $\pi^+\pi^+\pi^-$ invariant mass for the simulated events. The two main features are the $a_1(1260)/a_2(1320)$ region near 1.3 GeV/c^2 and the $\pi_2(1670)/\pi_1(1600)$ region near 1.6 GeV/c^2.

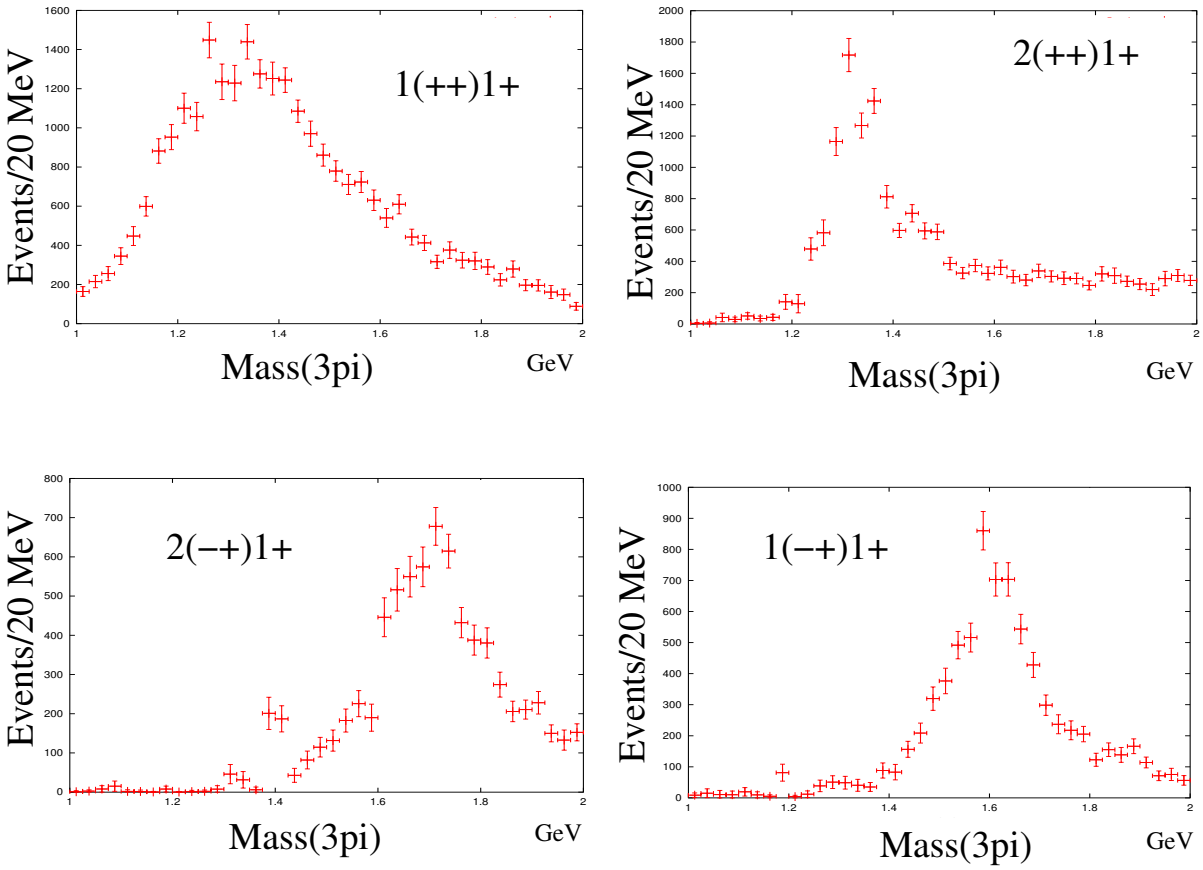

Figure 4: The PWA intensities resulting from the mass independent PWA fits of the simulated data. The $a_1(1260)$, $a_2(1320)$,$\pi_2(1670)$, and $\pi_1(1600)$ are exhibited in $1^{++}1^+$, $2^{++}1^+$, $2^{-+}1^+$, and $1^{-+}1^+$ partial waves, respectively.

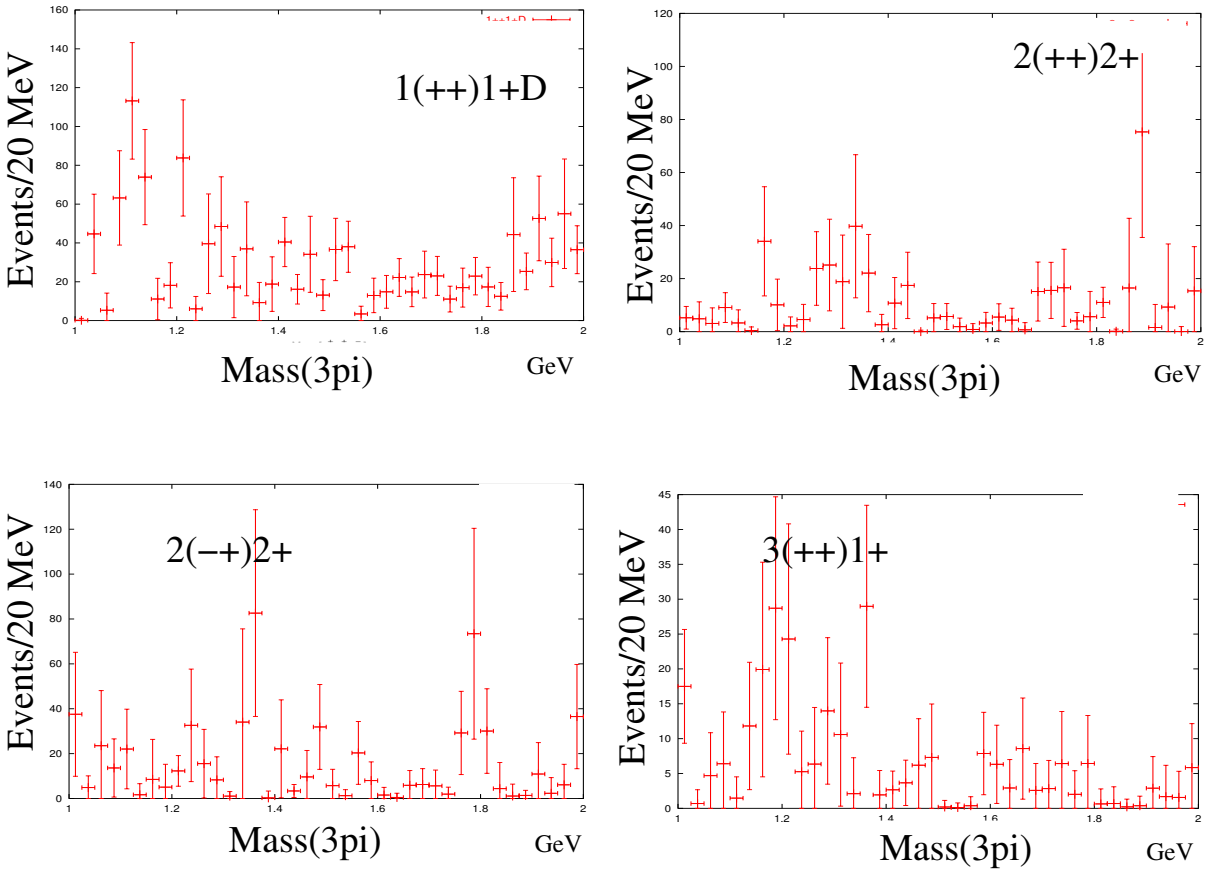

Figure 5: The PWA intensities resulting from the mass independent PWA fits of the simulated data. One expects not to observe resonance structure in these partial waves.

CLAS detector configuration (torus magnet at half maximum field and target moved one meter upstream of its standard position) in order to maximize acceptance for the reaction $\gamma p \to n\pi^+\pi^+\pi^-$ in the low-t region. The experiment was limited to a total of 8 days run time. The analysis of these data is now underway, and early results have shown the feasibility of using CLAS for meson spectroscopy. With a photon beam energy in the range of 5 to 6 GeV, we were able to readily photo-produce states of masses up to about 2 GeV/c^2. This allows us to access the exotic 1^{-+} candidates states that have been recently observed [3, 4].

We have led the development and implementation of the energy-independent partial wave analysis for our experiment. First partial wave analysis on a small subset of our data are shown for the benchmark reaction $\gamma p \to p\pi^+\pi^-$ in Figure 6. The accepted $\pi^+\pi^-$ invariant mass is shown in Figure 6a. The results of the partial wave analysis are shown in Figure 6b-d. In Figure 6b the $\rho(770)$ shows up clearly in the $J^{PC}|M| = 1^{--}|1|$ partial wave as expected for helicity conservation in the t-channel. Two other partial wave intensities are shown: in Figure 6c, the non-helicity conserving ρ partial wave; and in Figure 6d, the isotropic $J^{PC} = 0^{++}$ partial wave. Note that there appears to be a slight ambiguity in the analysis between the $1^{--}|1|$ and 0^{++} in the mass range above 1 GeV, that is events with hard zeros in the 0^{++} distribution leak into the 1^{--} distribution.

We have tracked this problem down due to backgrounds from Δ's and N^*'s which are produced at one of the πp vertexes. Figure 7 exhibits the $\pi^- p$ invariant mass for these data. The $\Delta^0(1232)$, $N(1520)/N(1535)$, and $\Delta^0(1620)$ are clearly visible in the mass spectrum. The $\Delta^{++}(1232)$ (not shown) is also cleanly produced. While it is relatively easy to cut out the $\Delta(1232)$ without much loss in statistics, it is much more difficult to cleanly cut the higher mass Δ's and N^*'s. The effects of this baryon background on the phi (ϕ_{TY}) angular distribution[2] in the $\pi^+\pi^-$ Gottfried-Jackson Frame can be seen in the "V" plot of Mass($p\pi$) vs ϕ_{TY}. Figure 8a shows the $\pi^- p$ "V" plot for accepted $\gamma p \to p\pi^+\pi^-$ data. The corresponding ϕ_{TY} distribution is shown in Figure 8b. A clear linear relationship is exhibited. This figure shows that events from different Δ's and N^*'s add to the structure of the angular distribution. This is a pure kinematic effect as can be seen in the similar "V" plot for phase space Monte Carlo events(See Figures 9a and 9b). The same Monte Carlo events subjected to the CLAS simulation (GSIM) are shown Figures 10a and 10b. It is interesting to note that one can turn this situation around, that is, a $\pi\pi$ resonance of high spin can have narrow structures in the ϕ_{TY} angular distributions which could result in a kinematic reflection of resonance-like structure in the $p\pi$ invariant mass distribution.

At beam energies of 5 GeV the data are plagued by this baryon background pollution. Care must be taken to try to clean and cut out the baryon background before performing the PWA, or one must include the baryon background in the PWA. In the results that follow, both approaches have been successfully developed and employed.

[2]The Treiman-Yang angle is the ϕ in the Gottfried-Jackson Frame.

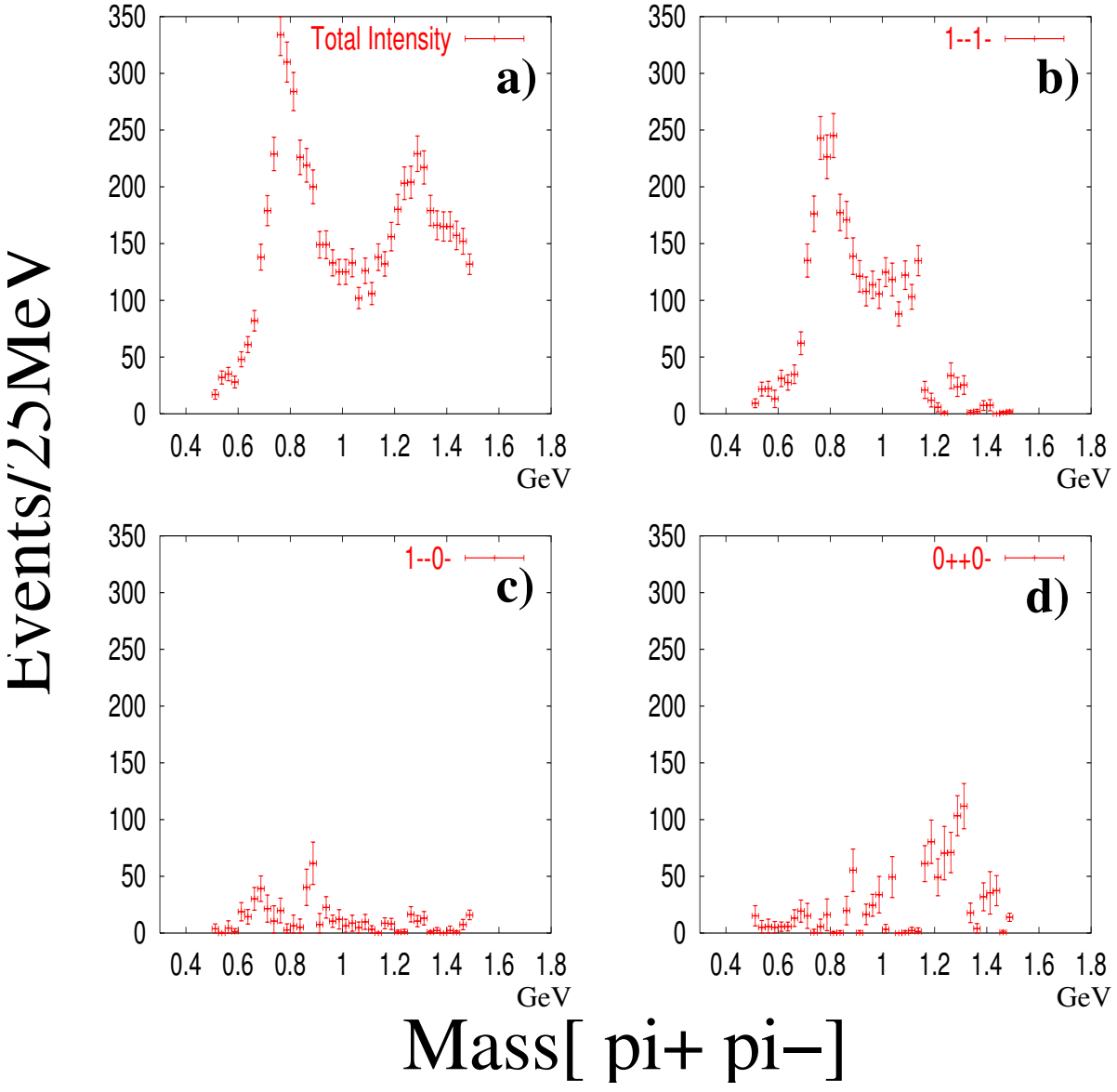

Figure 6: The reaction $\gamma p \to p\pi + \pi^-$. Preliminary mass independent partial wave analysis results from E01-017: a) The total accepted $\pi^+\pi^-$ mass spectrum, b) the partial wave intensity for $J^{PC}|M| = 1^{--}1$, c) the partial wave intensity for $J^{PC}|M| = 1^{--}0$, d) the partial wave intensity for $J^{PC}|M| = 0^{++}0$. Each data point in mass represents an independent partial wave analysis.

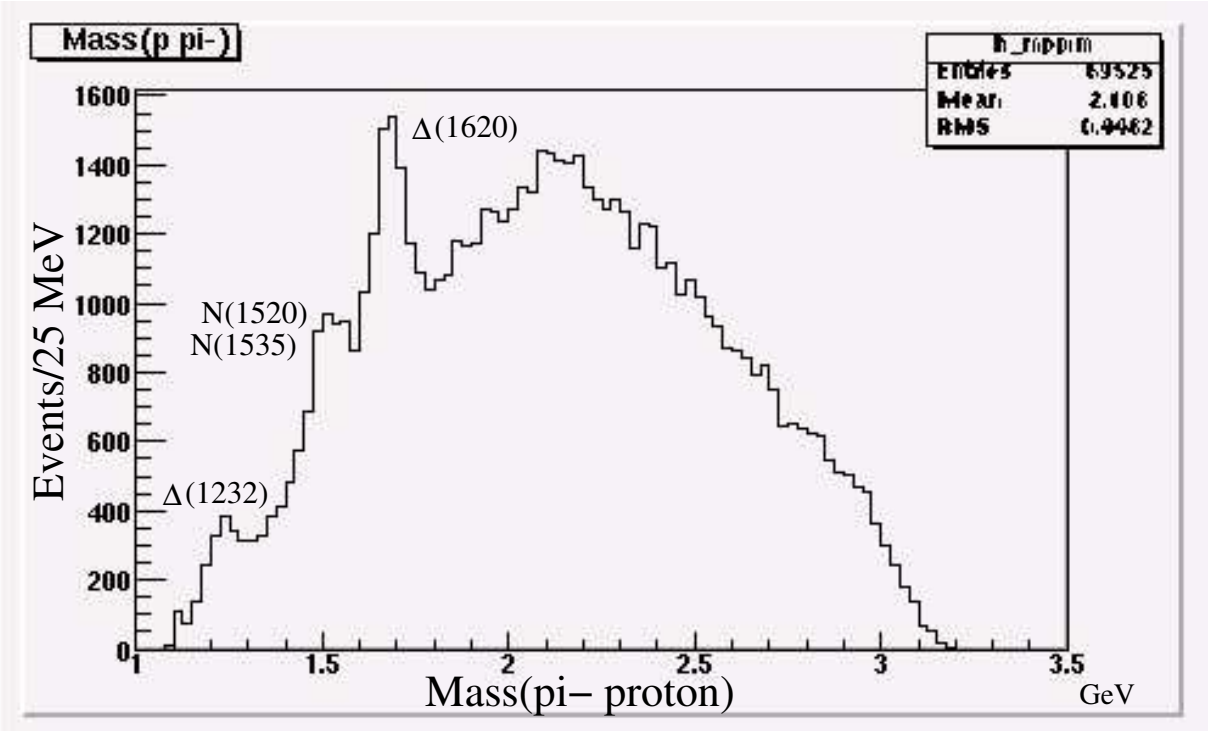

Figure 7: The accepted $\pi^- p$ invariant mass from the reaction $\gamma p \to p\pi^+\pi^-$.

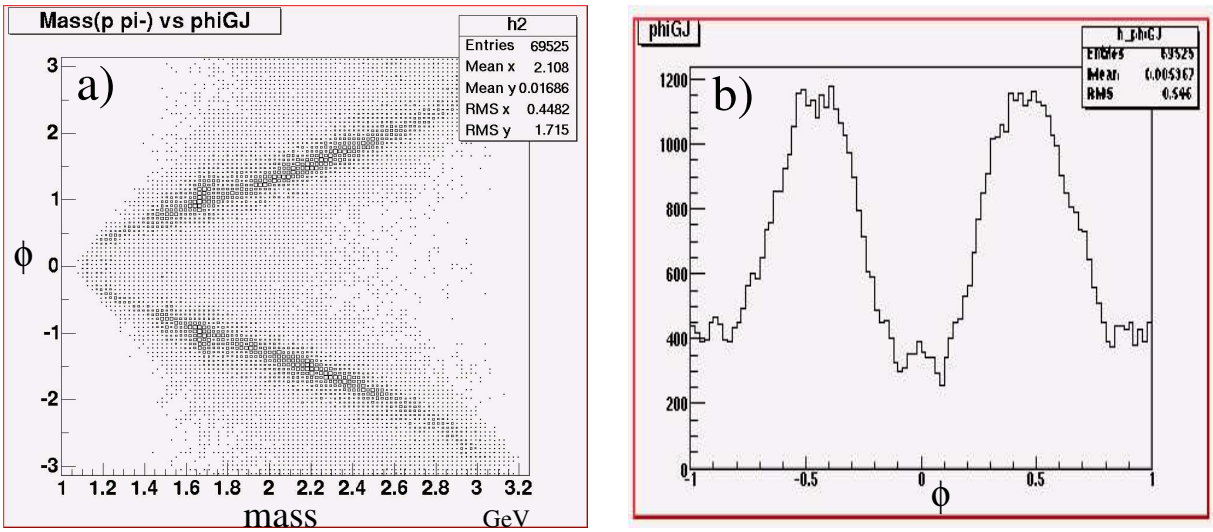

Figure 8: Experimental results for $\gamma p \to p\pi^+\pi^-$: a) ϕ_{TY} vs Mass($\pi^- p$), b) ϕ_{TY}/π. Not corrected for acceptance.

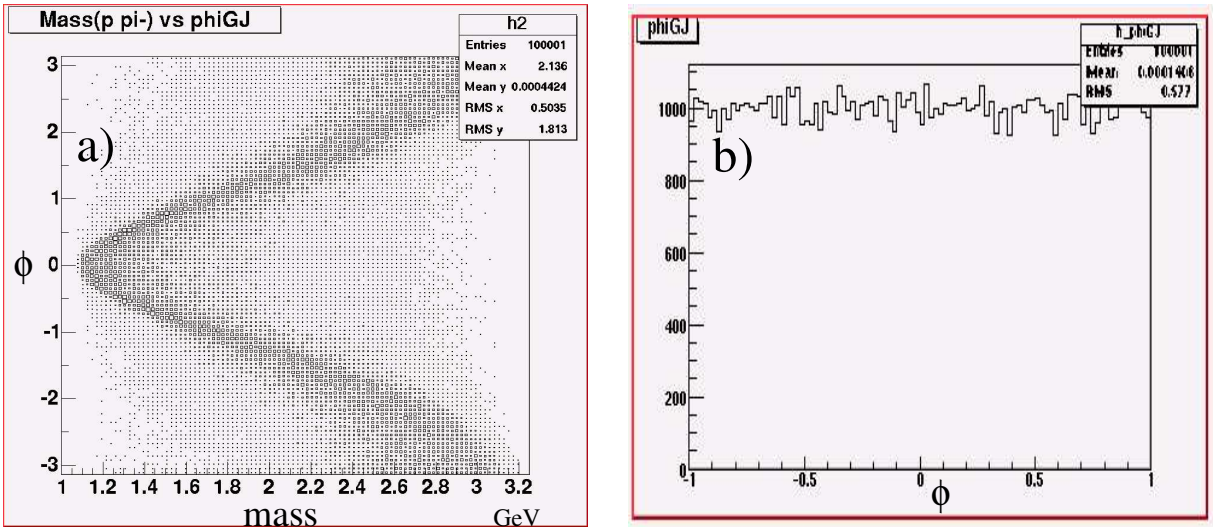

Figure 9: Monte Carlo results for $\gamma p \to p\pi^+\pi^-$: a) ϕ_{TY} vs Mass($\pi^- p$), b) ϕ_{TY}/π. Before CLAS simulation.

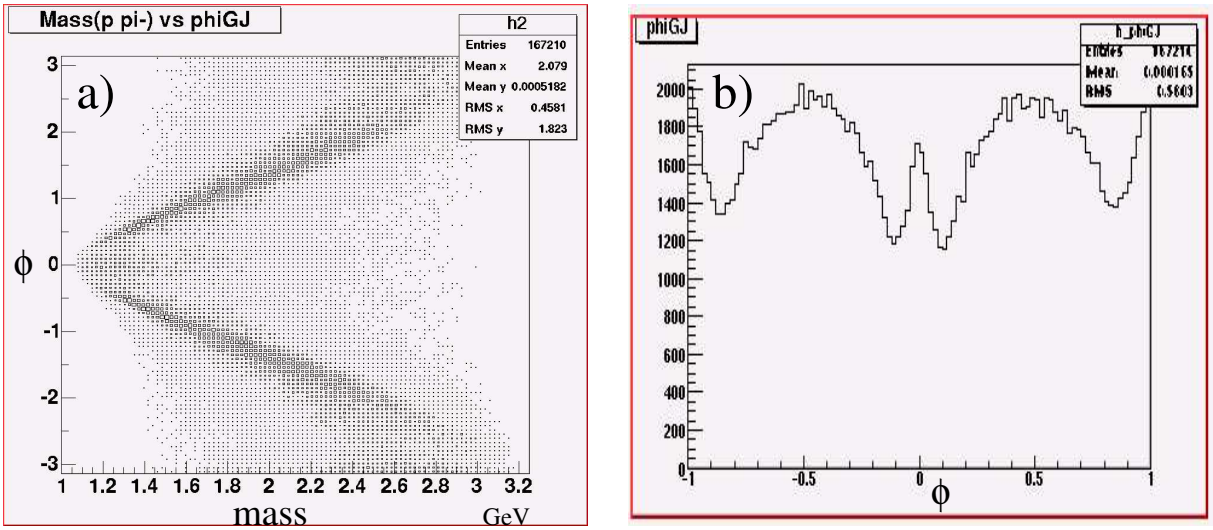

Figure 10: Accepted Monte Carlo results for $\gamma p \to p\pi^+\pi^-$: a) ϕ_{TY} vs Mass($\pi^- p$), b) ϕ_{TY}/π. After CLAS simulation.

$\gamma p \to p\pi^+\pi^-\pi^\circ$

For the reaction $\gamma p \to p\pi^+\pi^-\pi^0$ the three charged particles were measured in CLAS, while the π^0 was identified and measured from missing four-momentum. Figure 11 shows the accepted $\pi^+\pi^-\pi^\circ$ invariant mass. The main features include: the omega meson at 0.782 GeV/c^2, the $a_1(1260)/a_2(1320)$ near 1.3 GeV/c^2, and a broad peak just above 1.6 GeV/c^2 which is in the mass region where an exotic 1^{-+} meson has been observed[35]. This reaction has considerable background from baryon resonances decaying to $p\pi$ through t-channel exchange processes. For the partial wave analysis, this background was included as an interfering background, with the baryon resonance decay modeled as an S-wave decay. More sophisticated descriptions of the background did not significantly improve the results. A total of 28 meson waves and 21 background (baryon) waves were included, and are listed in Table 6. Many other waves were tried in the partial wave fits, and were determined to be very small. The preliminary results of the $\pi^+\pi^-\pi^\circ$ partial wave analysis for the isoscalar 1^{--}, the exotic isovector 1^{-+}, isovector 1^{++}, and isovector 2^{++} partial waves are shown in Figure 12. There is clear evidence for the photoproduction of the 1^{++} $a_1(1260)$ as well as the 1^{--} $\omega(1650)$. There is some evidence for production of the 2^{++} $a_2(1320)$ as well. In addition, there is a strong signal that corresponds in mass and width to the exotic 1^{-+} $\pi_1(1600)$. Interestingly, there is a strong signal near 2 GeV/c^2 in the exotic 2^{+-} partial wave which may indicate the presence of a newly observed exotic state, shown in Figure 13.

J^{PC}	M^ϵ	**L**	**Isobars**
1^{++}	$0^+, 1^\pm$	$0, 2$	$\rho(770)$
1^{--}	$0^-, 1^\pm$	1	$\rho(770)$
1^{-+}	$0^-, 1^+$	1	$\rho(770)$
2^{++}	$0^-, 1^+$	2	$\rho(770)$
2^{-+}	$0^+, 1^\pm$	0	$f_2(1270)$
2^{-+}	0^+	2	$f_2(1270)$
2^{-+}	$0^+, 1^\pm$	$1, 3$	$\rho(770)$
2^{+-}	0^-	2	$\rho(770)$
3^{--}	$0^-, 1^+$	3	$\rho(770)$
3^{++}	$0^-, 1^\pm$	1	$f_2(1270)$
4^{++}	$0^-, 1^-$	3	$f_2(1270)$

Baryon resonance	$M_\rho{}^\epsilon$
$\Delta^{++}(1232)$	$0^\pm, 1^\pm, -1^\pm$
$\Delta^{+}(1232)$	$0^\pm, 1^\pm, -1^\pm$
$N^{*+}(1650)$	$0^\pm, 1^\pm, -1^\pm$
$N^{*0}(1650)$	$0^+, 1^-, -1^+$

Table 6: Waves included in the PWA fit of $\gamma p \to \pi^+\pi^-\pi^0 p$

$\gamma p \to n\pi^+\pi^+\pi^-$

From the same data run the reaction $\gamma p \to \pi^+\pi^+\pi^- n$ was studied. The three charged pions were measured in CLAS, while the neutron was identified and measured from

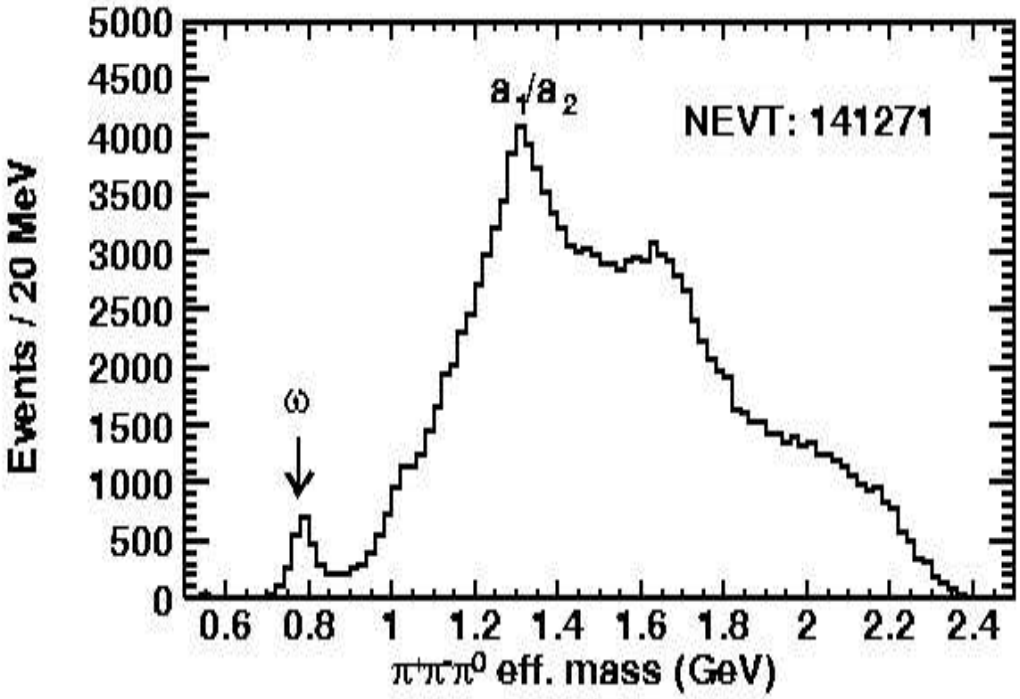

Figure 11: The reaction $\gamma p \to p\pi^+\pi^-\pi^\circ$: the accepted $\pi^+\pi^-\pi^\circ$ invariant mass.

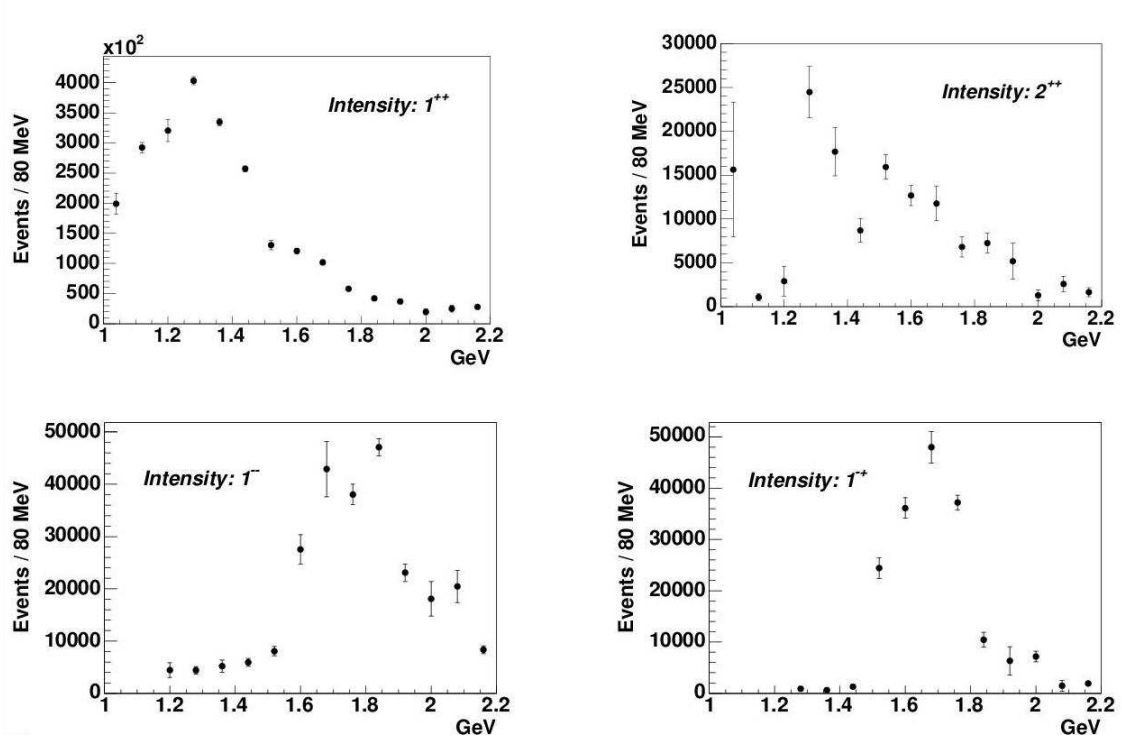

Figure 12: Partial wave decomposition of the reaction $\gamma p \to \pi^+\pi^-\pi^0 p$ (a) $J^{PC} = 1^{++}$ isovector, (b) $J^{PC} = 2^{++}$ isovector (c) $J^{PC} = 1^{--}$ isoscalar (d) $J^{PC} = 1^{-+}$ isovector.

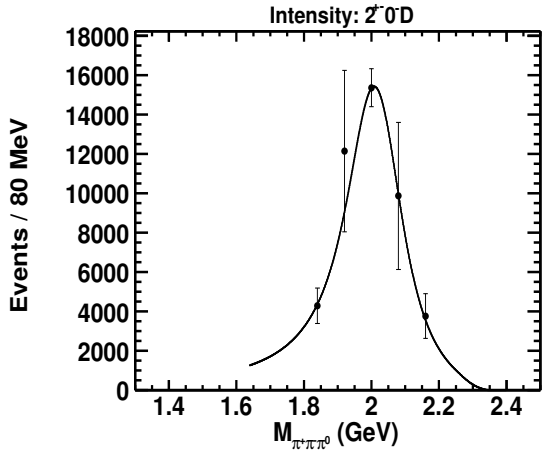

Figure 13: The exotic 2^{+-} partial wave of the reaction $\gamma p \to \pi^+\pi^-\pi^0 p$.

J^{PC}	m^{ϵ}	L	Isobar	# Waves
0^{-+}	0^{+}	0	σ	1
0^{-+}	0^{+}	1	$\rho(770)$	1
1^{++}	0^{+}, $1^{\pm}$	0,2	$\rho(770)$	6
1^{++}	0^{+}, $1^{\pm}$	1	σ	3
1^{-+}	0^{-}, $1^{\pm}$	1	$\rho(770)$	3
2^{++}	0^{-}, $1^{\pm}$, $2^{\pm}$	2	$\rho(770)$	5
2^{-+}	0^{+}, $1^{\pm}$	1,3	$\rho(770)$	6
2^{-+}	0^{+}, $1^{\pm}$	2	σ	3
2^{-+}	0^{+}, $1^{\pm}$	0,2	$f_2(1270)$	6
Background				

Table 7: Partial waves included in the fit of $\gamma p \to n\pi^+\pi^+\pi^-$

missing four-momentum. Laboratory angle cuts on the pions, as well as the selection of low t events, greatly reduce the baryon resonance background. Figure 14 shows various distributions of the data: the $t\prime$ distribution, the missing neutron mass, and di-pion effective masses.

The preliminary PWA results are shown in Figure 15; waves included in the fit are listed in Table 7. While these results are very preliminary, there is a very clear signal for the 2^{++} $a_2(1320)$. There is some evidence for photoproduction of the 1^{++} $a_1(1260)$ and also the 2^{-+} $\pi_2(1670)$. There is some strength in the exotic $J^{PC} = 1^{-+}$ partial wave near 1600 MeV/c^2, but it is not conclusive. It is interesting to note that the results of this PWA are remarkably similar to those of the earlier PWA simulation study.

$\gamma p \to pp\bar{p}$

The proton-antiproton system has had a rich history spanning more than thirty years. Initially, the $p\bar{p}$ system attracted much interest due to theoretical predictions of exotic matter. These predictions included: nucleon-antinucleon states that are loosely bound in a molecule-like structure called quasi-nuclear baryonium, and tightly-bound multi-quark baryonium ($qq - \bar{q}\bar{q}$) which have favored decays to nucleon-antinucleon final states. In the early 1970's, there were claims of a unusually-narrow meson resonance with a mass of 1.93 GeV/c^2 [36, 37]. It was believed that this particle was not an ordinary meson, and that it would couple to the proton-antiproton system. There were then claims that experiments found the narrow resonance in proton-antiproton scattering experiments [38, 39, 40, 41]. Also, in the late 1970s there were claims of additional higher mass narrow resonances at 2.02 and 2.20 GeV/c^2 in the proton-antiproton system [42, 41, 43]. However, follow up experiments did not make such claims[44, 45], and until recently, the debate had died out. In 1997, CERN refuted their earlier claims of the 1.93 and 2.02 GeV/c^2 resonances, yet in 1999, a

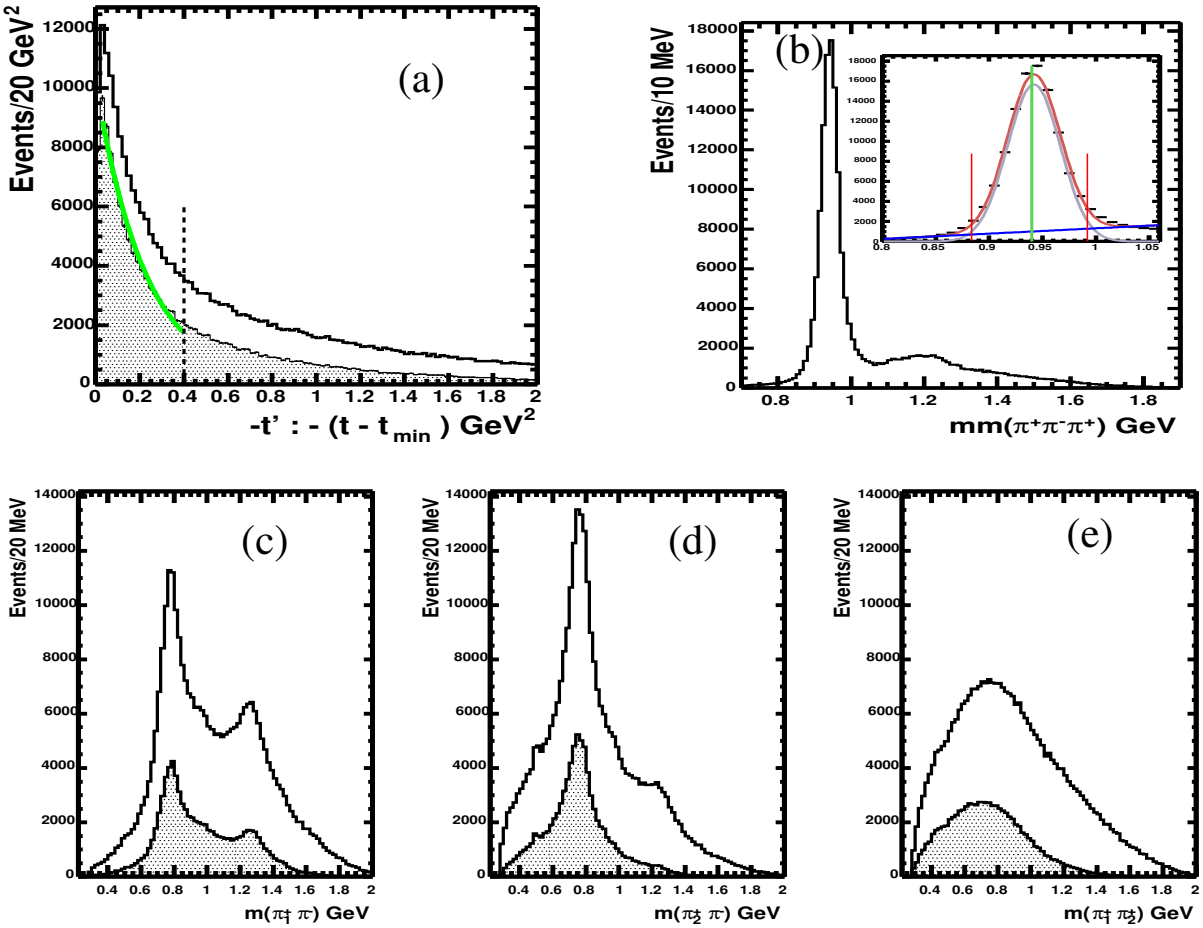

Figure 14: Various distributions of the reaction $\gamma p \to \pi^+\pi^+\pi^-n$ at 5.2 GeV. (a) $t\prime$ distribution. Events to the left of the dotted line were selected for the PWA. The shaded area has cuts on the pion laboratory angles described in the text. (b) Missing mass off of $\pi^+\pi^+\pi^-$ showing the missing neutron. (c) Mass of the π^- and slow π^+ showing both the ρ and $f_2(1270)$ isobars. (d) Mass of the π^- and fast π^+. (e) Mass of $\pi^+\pi^+$. (c),(d), and (e) shaded areas are events selected for the final partial wave analysis.

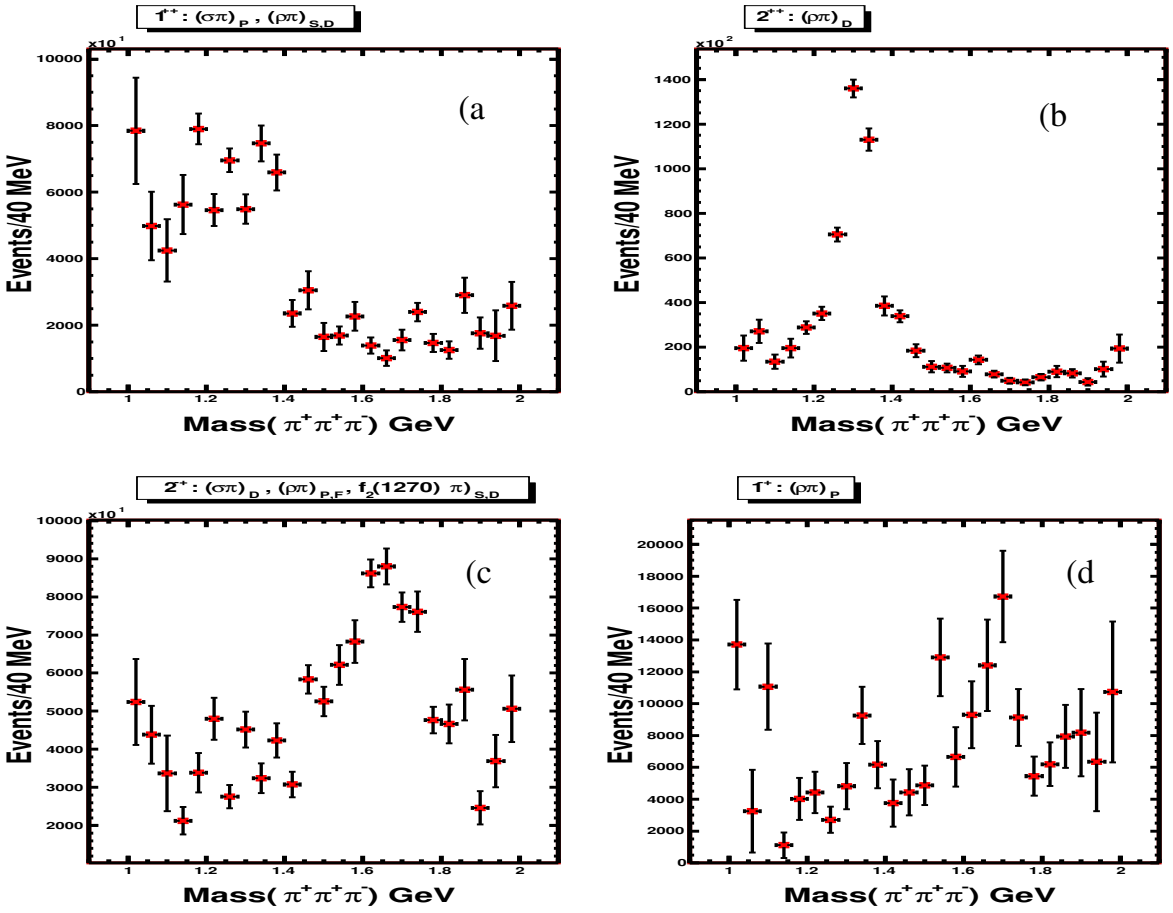

Figure 15: Partial wave decomposition of the reaction $\gamma p \to \pi^+\pi^+\pi^-n$. (a) $J^{PC} = 1^{++}$ partial wave. (b) 2^{++} partial wave. (c) 2^{-+} wave. (d) Exotic 1^{-+} wave.

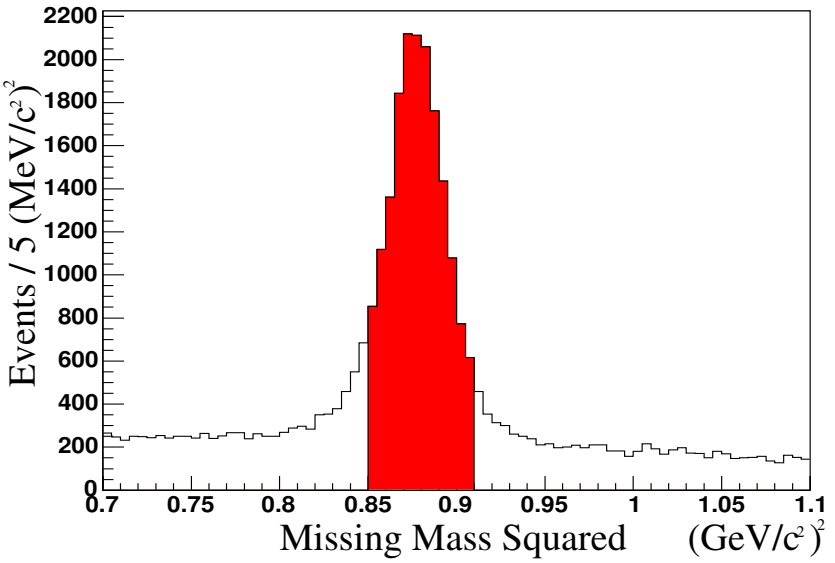

Figure 16: The reaction $\gamma p \to pp\bar{p}$: missing mass squared off two protons.

reanalysis of the CERN data confirmed the existence of the 2.02 and 2.2 GeV/c^2 resonances. Recently the BES collaboration has claimed to observe a narrow baryonium state with a mass near the proton-antiproton mass threshold, which decays to proton-antiproton[46]. Presently, the only well-known particle that decays to proton-antiproton is the J/ψ particle, with a mass of 3.097 GeV/c^2 [47]. Most of the past experiments involved proton-antiproton scattering or pion production. Recently Jefferson Laboratory has provided the first look at the proton-antiproton system through photoproduction.

In the recent CLAS high-energy photon data run, nearly five thousand exclusive $\gamma p \to pp\bar{p}$ events were observed where all final state particles were identified in the CLAS spectrometer. However, in CLAS there are regions of the detector where particles can go unmeasured. For example, the CLAS toroidal magnetic field bends negatively charged particles back toward the beam. Quite often, these particles end up going back into the beam-line, and are lost. To increase the exclusive data yield, the anti-proton was allowed to be identified via the missing mass.

Figure 16 shows the missing-mass-squared of events containing two identified protons. There is a prominent peak at a mass squared of 0.880 $(GeV/c^2)^2$, which is consistent with a missing antiproton. Selecting the events consistent with a missing antiproton [0.85 $(GeV/c^2)^2 \leq MM^2 \leq$ 0.91 $(GeV/c^2)^2$] yields approximately 17,100 $\gamma p \to pp(\bar{p})$ events.

Possible mechanisms which could describe the photoproduction of a proton-antiproton pair are diffraction/meson exchange, baryon exchange, and anti-baryon exchange. In

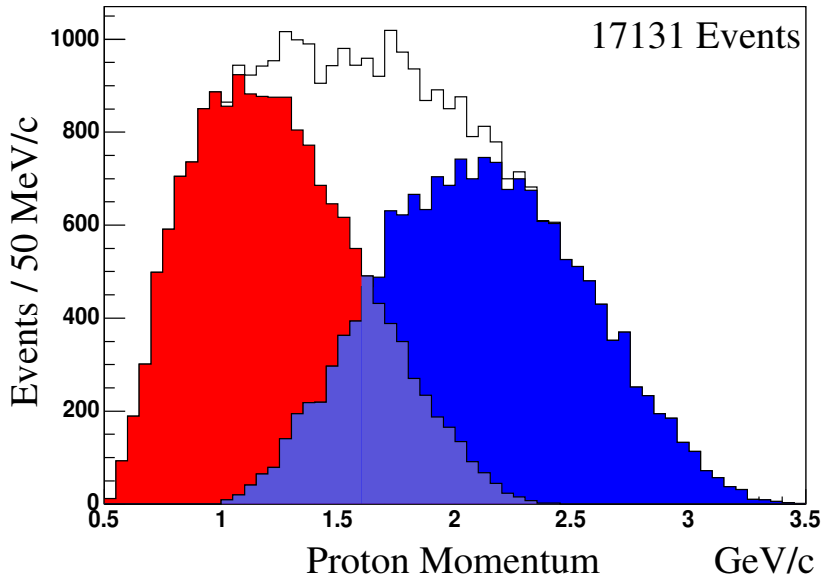

Figure 17: The reaction $\gamma p \to pp\bar{p}$: proton momentum distributions. In each event, whichever proton has less momentum is placed in the "slow" distribution (red/light-shaded) and the other goes into the "fast" distribution (blue/dark-shaded).

each process, an intermediate resonance may be produced. In meson exchange the photon transfers very little momentum to the target, but interacts with the exchanged meson to produce a resonance that decays to a fast forward-going proton-antiproton pair. In baryon exchange, the photon interacts with an exchanged baryon converting it to a fast forward-going proton, leaving behind a slow moving meson resonance at the target vertex which decays to a proton-antiproton pair. For anti-baryon exchange, the photon interacts with an exchange anti-baryon, converting it to a fast forward-going antiproton and leaving behind a resonance at the target vertex which decays to two protons.

The distinction of meson exchange and baryon exchange production is clouded by the two identical protons. Without information identifying which is which, the two mechanisms are nearly indistinguishable. A simple way to distinguish protons is to sort on the proton momentum. In the cases of meson and baryon exchange, one proton should be moving fast and in the forward direction, while the other proton is produced at or near the target vertex, receives very little momentum transfer from the beam, and is expected to be slow. Therefore, one can use the momentum of the two protons on an event by event basis and associate a $p_{fast}\bar{p}$ resonance with meson exchange and a $p_{slow}\bar{p}$ resonance with baryon exchange. In Figure 17, the proton momentum distribution is shown. The proton with the greatest magnitude

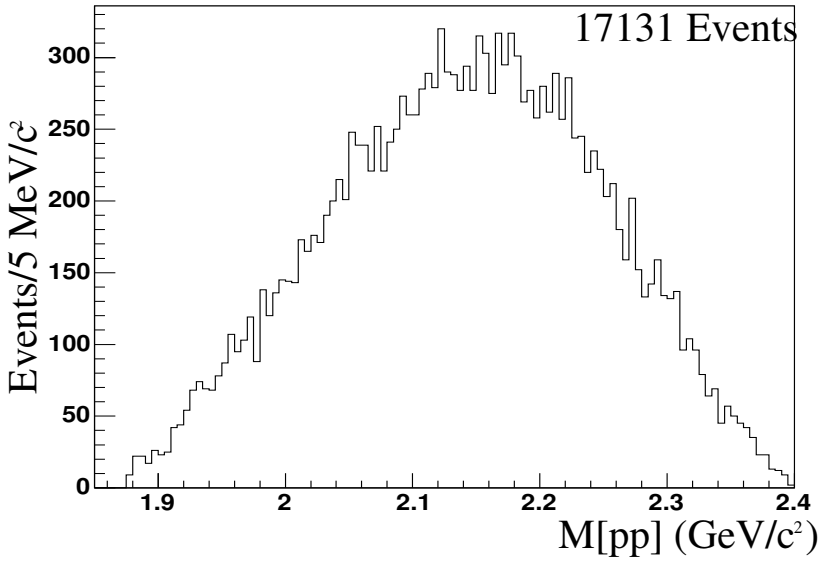

Figure 18: The reaction $\gamma p \to pp\bar{p}$: the accepted invariant mass distribution of the two protons.

of momentum is labeled as the fast proton, and the other proton is labeled as the slow proton. The light-shaded histogram shows the event by event distribution for the slow protons whereas the dark-shaded histogram is that for the fast protons.

The two proton invariant mass is shown in Figure 18. No obvious peaks or features are observed. In the invariant mass distribution of $p_{fast}\bar{p}$ (See Figure 19) there are no obvious structures indicating resonant nature. The invariant mass of $p_{slow}\bar{p}$ is shown in Figure 20. The distribution has some interesting structures, with a sharp rise at threshold and a possible narrow peak or dip near 2.0 GeV and broader peak at 2.04 GeV. While it is possible that these feature could be due to acceptance, preliminary Monte Carlo studies suggest otherwise and that the acceptance is smoothly varying as a function of the $p\bar{p}$ invariant mass. Current analysis plans include performing a partial wave analysis to search for resonant behavior in $p\bar{p}$ system.

$\gamma p \to \Delta^{++}\eta\pi^-$

One of the first signs of a $J^{PC} = 1^{-+}$ exotic meson candidate, now know as the $\pi_1(1400)$, was observed in the $\eta\pi^-$ channel in pion production [3]. Claims of an exotic meson decaying to $\eta\pi^-$ have had a rich and controversial history. Since photoproduction is expected to favor gluonic hybrid production, observation of or not of an exotic $\pi_1(1400)$ in $\eta\pi$ photoproduction would provide critical information regarding the nature of the $\pi_1(1400)$. Since CLAS does not identify neutral particles well, other

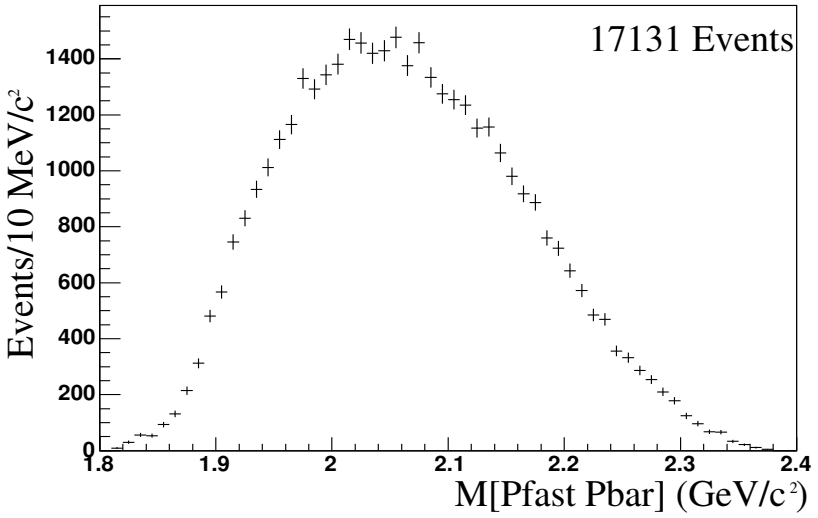

Figure 19: The reaction $\gamma p \to pp\bar{p}$: the invariant mass of the fast proton with the antiproton.

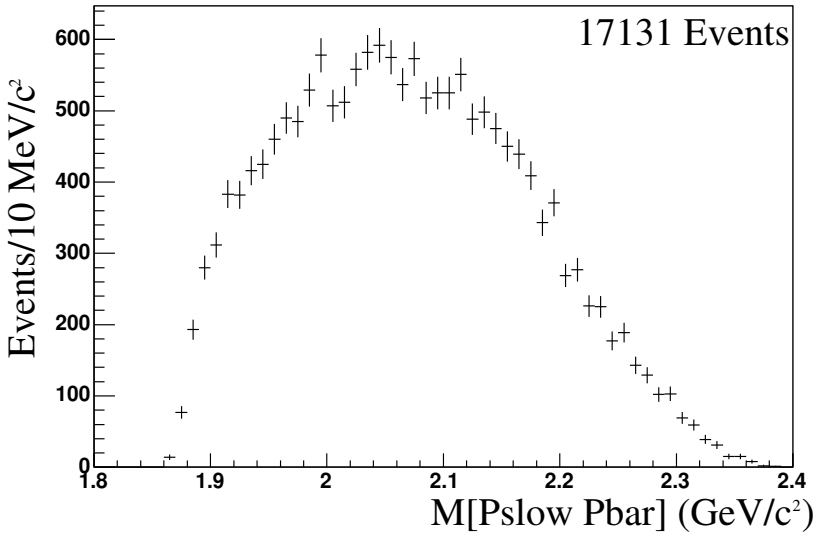

Figure 20: The reaction $\gamma p \to pp\bar{p}$: the invariant mass of the slow proton with the antiproton.

than via missing mass, it is very difficult to study reactions with two missing neutrals like $\gamma p \to n\eta\pi^+$. Efforts are underway to improve the utilization of the CLAS electromagnetic calorimeter for η and π^0 identification. On the other hand, we have explored the possibility of $\eta\pi$ meson production off of a recoiling Δ^{++}. Figure 21 shows the results of this study. The missing mass off of the $p\pi^+\pi^-$ system is shown in Figure 21a. The distribution exhibits a clear missing η signal. Selecting the η events as shown, Figure 21b displays the $p\pi^+$ invariant mass which exhibits a strong Δ^{++} signal. Figure 21c shows $\eta\pi^-$ invariant mass for both the η and Δ^{++} selections. The $a_2(1320)$ is clearly observed in the mass spectrum. This data corresponds to nearly 11,000 $\Delta^{++}\eta\pi^-$ events(after background subtraction) which is too small to partial wave analyze. Yet an order of magnitude more data, as requested later in the proposal, would provide enough statistics to explore the resonant nature of the $\eta\pi^-$ system and to search for the $\pi_1(1400)$ exotic.

5 Monte Carlo Acceptance Studies

Monte Carlo studies were conducted to find the optimal CLAS configuration for the proposed experiment. The goal was to maximize the acceptance for a few reaction topologies of interest. As a benchmark, we used reaction $\gamma p \to \pi^+\pi^-\pi^o p$ where a signal from the exotic 1^{-+} and, possibly, 2^{+-} states was seen in the g6c run of CLAS.

The phase-space Monte Carlo events were generated assuming the t-channel production with a slope $b = 3\ (GeV/c^2)^{-2}$. This number is based on the g6c data. To study the acceptance as a function of the 3π mass, the Monte Carlo events were generated in 10 MeV bins with 200 MeV step over the range from 1 GeV to 2 GeV.

In this study, we varied the magnetic field (torrus current) as well as Z pozition of the liquid hydrogen target. We assumed a target length of (18 cm). Standard CLAS GEANT-based Monte Carlo package `GSIM` was used for detector simulation. Track reconstruction was also done by means of a standard reconstruction program `a1`. For a given combination of the magnetic field and target configuration, an appropriate "link" file (required for pattern recognition) was generated with `SDA` software package.

A $\gamma p \to \pi^+\pi^-\pi^o p$ event was accepted if all 3 charged tracks were reconstructed. π^o meson was detected through a missing mass technique. Fig. 22 shows a typical distribution of the missing mass (with sign preserved). A gaussian fit of the π^o peak results in a resolution of $\sigma = 50\ MeV$.

Fig. 23 shows the experimental acceptance as a function of the $\pi^+\pi^-\pi^o$ mass for two Z positions of the target: at -100 cm (left) and at -75 cm(right). At each position, three values of the torrus current were tried: 1930 A, 2250 A and 3375 A. These values roughly correspond to the 50%, 60% and 78% of the full torus magnetic field. The maximum CLAS has run with has been at 78% of the full field. As one can see from Fig. 23, the best acceptance in the 1.6-2 GeV mass region is achived at half-field (1930 A) and with a target at -100 cm.

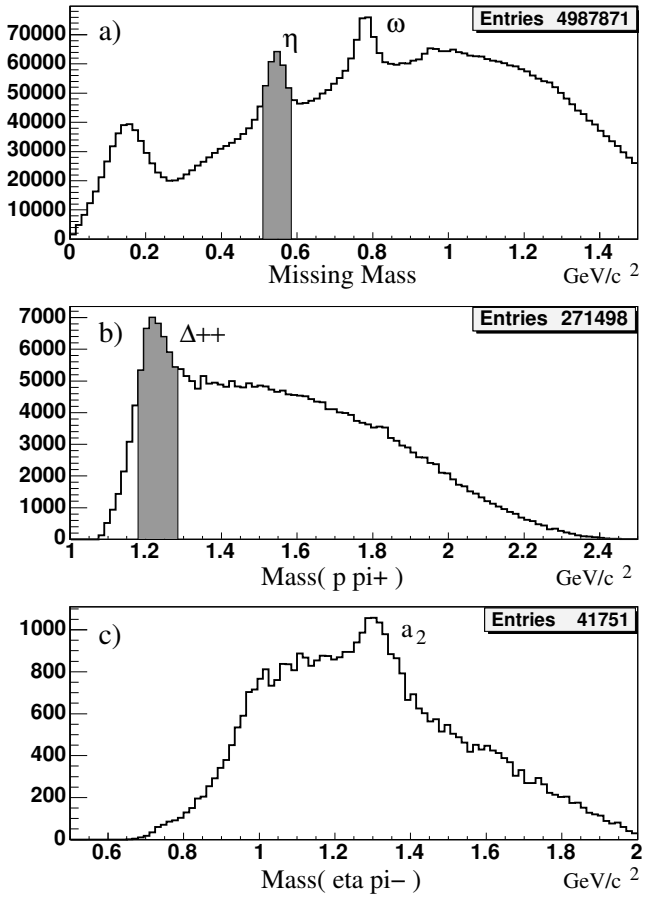

Figure 21: The reaction $\gamma p \to \Delta^{++}\eta\pi^-$: a) the missing mass of X in the reaction $\gamma p \to p\pi + \pi^-$ (X), b) Mass($p\pi^+$) for the η selection shown, and c) Mass($\eta\pi^-$) for the η and Δ^{++} selection shown.

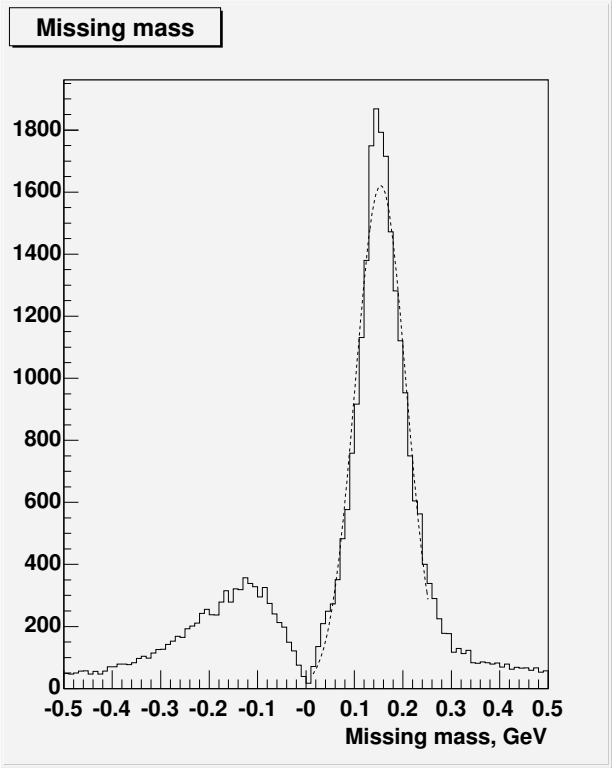

Figure 22: Missing mass distribution from Monte Carlo.

.

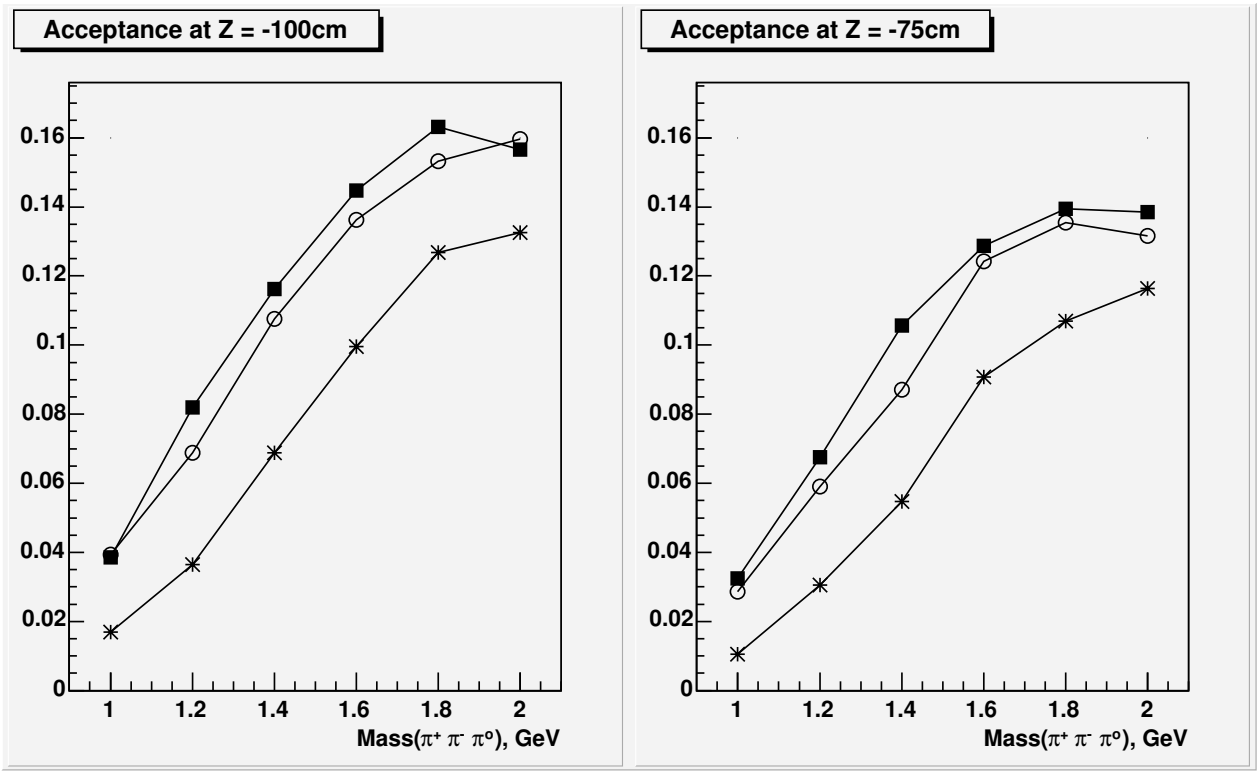

Figure 23: Acceptance as a function of 3π mass for target at -100 cm (left) and -75 cm (right). Torus current: 1930 A (closed squares), 2250 A (open circles), and 3375 A (stars).

6 Run Conditions

We will perform a high statistical partial wave analysis of meson spectroscopy data acquired using CLAS. We will study meson systems in the mass ranging from 1.0 to 2.3 GeV in reactions having three to four charged particles in the final state of the form:

$$\gamma\ p \to p\pi^+\pi^-\pi^0$$
$$\gamma\ p \to n\pi^+\pi^+\pi^-$$
$$\gamma\ p \to p\phi\eta \to pK^+K^-\eta$$
$$\gamma\ p \to n\phi\pi^+ \to nK^+K^-\pi^+$$
$$\gamma\ p \to n\pi^+\pi^-\pi^+\pi^-$$
$$\gamma\ p \to \Delta^{++}\eta\pi^- \to p\pi^+\pi^-\eta$$
$$\gamma\ p \to \Delta^{++}\omega\pi^- \to p\pi^+\omega\pi^-$$
$$\gamma\ p \to n\eta\prime\pi^+ \to n\pi^+\pi^-\eta\pi^+$$
$$\gamma\ p \to pK^{\pm}K^0\pi^{\mp}$$
$$\gamma\ p \to pp\bar{p}$$

The photon energy required to reach the production threshold for a meson X of mass m_X is (M_t is the proton target mass and M_r is the baryon recoil mass)

$$E_\gamma = \frac{{m_X}^2 + {M_r}^2 - {M_t}^2 + 2m_X M_r}{2M_t}$$

Therefore, with a 5-6 GeV photon beam we can reach up to 2.3-2.5 GeV in meson masses. However, since we need to populate enough phase space for the decay products of the mesons to be experimentally measurable, at least an extra 0.5 GeV from the threshold energy is required. For example, for the $\phi(1850)$ decays to be detected, it will be necessary for photon energies of around 5 GeV. Higher beam energies are desirable to isolate the baryon and meson decays in phase space. However, in the case of strangeness production, the number of strange baryons contributing to the background are less and better isolated than for $n\bar{n}$ backgrounds. In some cases, i.e., $K\bar{K}\pi$) decay channel, baryon backgrounds are not present.

The CLAS running conditions for this experiment will be similar to those proposed for the Θ^+ search off of the proton. The running conditions are summarized in table 8. The previous high energy real photon CLAS experiment, E01-1017 (g6c), ran photon rates of about 4 x 10^6 Hz using the high energy end of the tagger (or 5 x 10^7 Hz over the whole tagger range), a factor of two higher than most photon data runs. It should be noted that this flux limit was imposed by the operational limits of the CLAS start counter. A planed upgrade of the CLAS start counter system will allow to increase this flux by an order of magnitude(See section below on Accidentals).

E_{beam}	5-6 GeV - unpolarized photons
Target	40 cm LH2
B Field	1/2 B_{max}
trigger (CLAS)	2-3 charged particles, L2
Daq rate	$\sim$ 3 kHz
Run Time	1000 Hours

Table 8: Running Conditions.

The data rates for a meson resonance are estimated for the $\gamma p \to n\rho\pi$, $\gamma p \to p\pi_1(1600) \to n\eta'\pi^+$, and $\gamma p \to p\phi(1680) \to pK^+K^-\eta$ topologies. The detector acceptances was calculated using a phase space generator, a Geant 3 simulation of CLAS (GSIM) and the standard reconstruction CLAS software (a1). The CLAS simulation, GSIM, has been compared with several sets of CLAS data and is known to duplicate very well the detector characteristics. Finally, we use g6c data to obtain total reduction efficiencies, including rejection for accidentals and baryon resonance events.

The total cross section for $\gamma p \to \rho^0\pi^+$ ($\rho \to \pi^+\pi^-$) at 5.6 GeV photons is about 950 nb [48]. For approximately 4 events/μb/sec this yields 3.8 events/sec. The total accepted yield at 4% acceptance is appromimately 550 events/hour.

The reaction $\pi_1(1600) \to \eta'\pi$ has not been measured in photoproduction. We can estimate its rate based on hadroproduction data and predictions for photoproduction. BNL-E852 measured [49] the $\pi_1(1600)$ to have a strength about 1/10 of that of the a_2^- in pion production. Szczepaniak et al. [50] had predicted that the photoproduction cross section of the $\pi_1(1600)$ exotic will be about 5 to 10 times higher, therefore about half that of the a_2^-. W. Struczinski *et al.* had measured a $\gamma p \to n a_2^+$ cross section of about 700 nb at 4 GeV[48]. Assuming a $\pi_1(1600)$ branching ratio of 1/3 to $\eta'\pi$, we estimated a cross section of 115 nb for the reaction $\gamma p \to n\pi_1(1600) \to n\eta'\pi^+$. With an acceptance of 2% we expect a rate of approximately 33 events/hour.

The photoproduction $\phi\eta$ has never been observed before. Being one of the channels with the low cross section, we use it determine the neccesary runtime of our experiment. We estimated rates using theoretical predictions by Barnes, Black and Page [13]. Where they predict

$$\frac{Br(\phi\eta)}{Br(K^+K^-)} = 0.5$$

The cross section for K^+K^- photoproduction was measured at 45 GeV by the OMEGA collaboration [15]. They obtained a cross section of about 8 nb per 50 MeV mass bin. Our lower beam energy should increase the yield somewhat for resonance production so we estimate a cross section of 15 nb per 50 MeV bin for K^+K^- production which agrees with preliminary g6c values. The data will be sorted into ap-

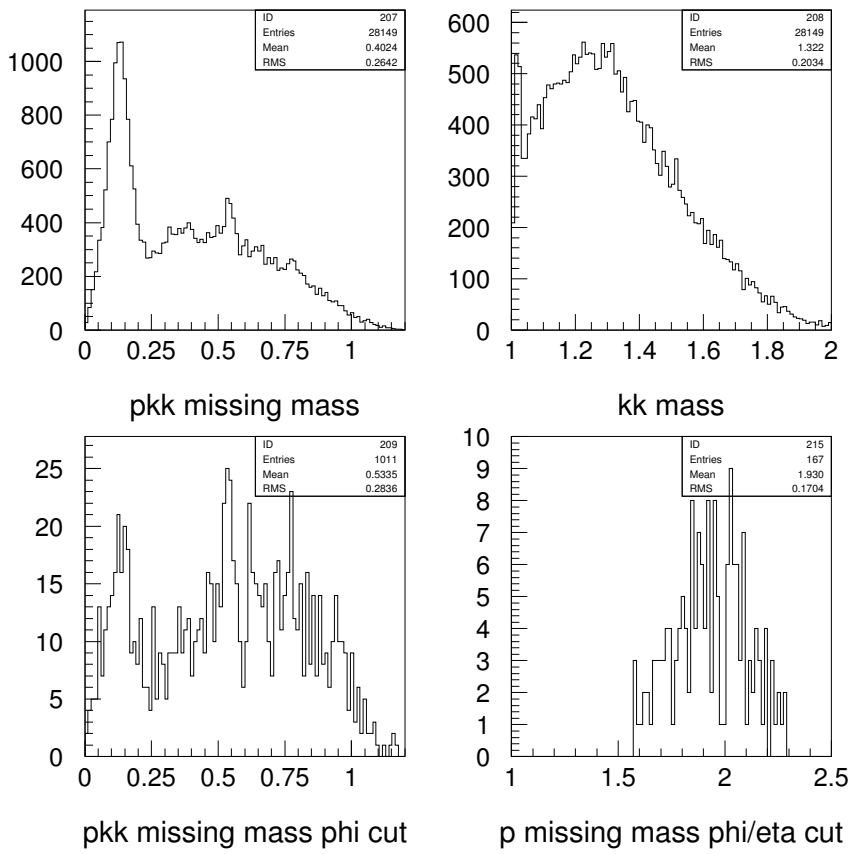

Figure 24: $\eta\phi$ data from g6c

proximately 20 mass bins. This will produce an event rate of 0.2 events/sec. Applying the CLAS acceptance (0.08) we will detect a total rate of 57 events/hour distributed over the whole mass range.

Shown are preliminary results from g6c in the search for a $\phi\eta$ resonance(See Figure 24). The pKK topology was studied where all three particles were observed in CLAS. Figure 24 shows the accepted $\phi\eta$ events. The statistics is too low to identify any resonance features. The total integrated luminosity of g6c was about $2.2 * 10^{36}\ cm^{-2}$. From the 167 observed events we can extimate (using an acceptance of 1.5% for this topology) a cross section of $167/(0.015 * 2.2 * 10^{36}) \approx 5\ nb$, that compares in general agreement with the former rate predictions.

Our goal is to obtain data samples which will enable us to perform an accurate partial-wave analysis. High statistics are critical to the ability to separate partial waves with good accuracy. Using a reasonable value of 3000 events per mass bin for a typical expected rate like those listed above, we arrive at a total beam-time request of

1000 hours. This will yield a factor of ten increase in the total integrated luminosity over that of g6c.

Accidentals

The CLAS photon run g6c ran at the highest photon rates as yet at Jefferson Laboratory. This experiment ran at a tagged photon flux of $5 \times 10^7/sec$, and at this rate each of the three elements of the Start Counter fired at a rate of about 200 kilohertz, while the total tagger OR rate was 10 Megahertz. For the physics program of g6c, only the top 12 T-counters of the tagger were used; this OR rate was approximately 1 Megahertz. A asynchronous trigger coincidence was formed between the Start Counter OR and the tagger OR, with a gate of about 15 nanoseconds. This coincidence was then put in with a coincidence of the CLAS time-of-flight counters, with a sector multiplicity of 2 and a gate of about 100 nanoseconds to form the Level 1 trigger. These triggers were subsequently processed by a crude sector tracking algorithm (Level 2) to form the data acquisition trigger. This trigger rate was approximately 1.5 kilohertz.

The accidental trigger rate of a two-component coincidence for individual rates f_1 and f_2, with a gate of Δt is approximated by

$$Rate \sim \Delta t f_1 f_2$$

G6c ran with 2 of 3 Start Counter elements in coincidence (15 nanoseconds) with the high energy end of the tagger, which gives an accidental trigger rate of order 10 hertz. However, much of the background can also be correlated hits in the Start Counter from untagged photons: this rate can be of the order of 10^5. It is this rate that is then put in coincidence with the CLAS detectors, for example time-of-flight multiplicity, with a 100 nanosecond gate.

The triggering concept proposed here is a bit different. The new Start Counter envisioned is nearly hermetic and finely segmented with approximately 100 channels, so we may trigger on Start Counter multiplicity ≥ 3, which cuts out pair production and limits the trigger to $E_\gamma > 0.5\ GeV$, and with a tight time gate as the Start Counter is small and just a few centimeters from the target. For accidental rate estimates we extrapolate the Geant simulation of Guidal, Marchand, and Smith. We thus estimate Start Counter rates to be about 8 MHz, 90% from Compton scattering and 10% from pair production. Thus the single counter rate is 80 kHz. In addition, we have measured Start Counter rates from g6c; these rate estimates are consistent. The 3-fold accidental coincidence is estimated to be

$$Rate \sim (5 \times 10^{-9})^2 (100^3)(8 \times 10^4)^3 \sim 12800.$$

Thus we have a 13 kHz accidental rate *without the tagger in the trigger.* To this we add CLAS time-of-flight multiplicity = 3. The time-of-flight singles rate is about 6 kHz under these conditions. A three fold coincidence with a 100 ns gate

$$Rate \sim 288^3(10^{-7})^2(6\times10^3)^3 \sim 50000$$

Adding these two in coincidence gives a Level 2 accidental trigger rate of order 100 Hz. If the CLAS time-of-flight multiplicity is relaxed to 2, the accidental rate will increase to about 400 Hz.

The 3-prong rate ($\sim$ 90 $\mu barns$) is estimated to be of the order of 12 kilohertz, but includes *desirable physics events*. This rate will be put in coincidence with the CLAS time-of-flight multiplicity, which includes geometric efficiency, and is of the order of 5%, for a total real trigger rate of order 1 kilohertz.

7 Summary

One of Jefferson Lab most important missions is the study of QCD at intermedate energies. Meson spectroscopy is one of the leading ways to study QCD at the confinement scale. Exotics, Hybrids, and Strangeonia are poorly known, and they represent the next frontier in hadronic physics. The spectroscopy of mesons in the 1 to 2 GeV/c^2 mass range will provide insight into these new forms of hadronic matter, and thus aid in the study of QCD at the realm of confinement. Jefferson Lab offers an unique opportunity to undertake the study of meson spectroscopy at intermediate energies. And current studies at CLAS are showing the feasibility of using CLAS as a meson spectrometer for few-body final states. Motivated by these and recent experimental results for gluonic hybrid meson candidates and from recent theoretical Lattice QCD and Flux-tube model calculations, We propose to search for gluonic hybrid mesons utilizing a high energy photon beam at CLAS. Given the current limited acceptance of CLAS, the present proposal will concentrate on important final states but with the focus on channels with a limited number of three to four charged particles in the final state. A 1000 hours run at the highest CEBAF energy (nominally 6 GeV) will produce enough statistics for a complete partial wave analysis of these reactions.

References

[1] N. Isgur, R. Kokoski, and J. Paton, *Phys. Rev. Lett.* **54**, 869 (1985).

[2] P. Lacock, et.al.(UKQCD Collaboration), *Phys. Lett.* **B401**, 308 (1997).

[3] D. R. Thompson et. al. (BNL-E852 Collaboration,) *Phys. Rev. Lett.* **79**, 1630 (1997).

[4] G. S. Adams et. al. (BNL-E852 Collaboration), *Phys. Rev. Lett.* **81**, 5760 (1998).

[5] See contributions from both A. V. Popov and D. V. Amelin, *9th International Conference on Hadron Spectroscopy: HADRON01* Protvino, Russia 2001.

[6] F. Close and P. Page, *Phys. Rev.* **D52**, 1706 (1995).

[7] A. Szczepaniak and M. Swat, *Phys. Lett.* **B516**, 72 (2001).

[8] N. Isgur and J. Paton, *Phys. Rev.* **D31**, 2910 (1985).

[9] GlueX/Hall D Collaboration *The Hall D Project Design Report* 38 (2000).

[10] T. Barnes, F. E. Close, and E.S. Swanson, *Phys.Rev.* **D52** 5242 (1995).

[11] G. R. Blackett, et al, *arXiv.org e-Print Archive* **hep-ex/9708032** (1997).

[12] S. U. Chung, *Brookhaven Report* **BNL-QGS-97-041** (1995).

[13] T. Barnes, N. Black and P.R. Page, *arXiv.org e-Print Archive* ,**Nucl-th/0208072** (2002).

[14] D. Bisello, *et al.*, *Z. Phys.***C52**, 227 (1991); J. Buon, et al., *Phys. Lett.***118B**,221 (1982).

[15] M. Atkinson, *et al.*,*Nucl. Phys.***B231**, 1 (1984).

[16] F. Mane et al., (DM1), Phys. Lett. 112B, 178 (1982).

[17] J.M. Link, et al.(FOCUS),*arXiv.org e-Print Archive* **hep-ex/0208027** (2002).

[18] F. Mane et al., (DM1),*Phys. Lett.***99B**, 261 (1981).

[19] B. Delcourt, et al., (DM1)*Phys. Lett.***99B**, 257 (1981)

[20] P.M.Ivanov, et al., *Phys. Lett.* **107B**, 297 (1981).

[21] D. Bisello, et al., (DM2) *Z. Phys.* **C39**, 13 (1988).

[22] J. Buon, et al., (DM1) *Phys. Lett.* **118B**, 221 (1982).

[23] A. Antonelli, et al., (DM2) *Z. Phys.* **C56**, 15 (1992).

[24] D. Aston, et al., *Phys. Lett.* **104B**, 231 (1981).

[25] M. Atkinson, et al., *Z. Phys.* **C27**, 233 (1985).

[26] J. Busenitz, et al., *Phys. Rev.* **D40**, 1 (1989).

[27] A. Donnachie and P.V. Landshoff, *Phys. Lett.* **B348**, 213 (1995).

[28] , P.D.B. Collins, and A.D. Martin, *Rep. Prog. Phys.***335**, 45 (1982).

[29] Partical Data Group, *Phys. Rev.* **D66**, 1 (2002).

[30] P. Eugenio, Int. J. Mod. Phys. A **18**, 487 (2003).

[31] James, F., *CERN Program Library Long Writeup* **D506 Ver.94.1** (1994).

[32] Orear, Jay, *Notes on Statistics For Physicists, Revised* **CLNS 82/511** (1982).

[33] Chung, S. U., *Brookhaven Report* **BNL-QGS-93-05** (1995).

[34] GlueX Collaboration *The Hall D Project Design Report* Chapter 10 (2000).

[35] BNL-E852 Collaboration (Chung, S. U., et al.) *Phys. Rev.* **D65** 072001 (2002).

[36] M.N. Focacci *et. al.,* Phys. Rev. Lett. 17, 890(1966).

[37] D. Cline *et. al.,* Phys. Rev. Lett. 17, 1268(1968).

[38] A.S. Carroll *et. al.,* Phys. Rev. Lett. 32, 247(1974).

[39] T.E. Kalogeropoulos and G.S. Tzanakos Phys. Rev. Lett. 34, 1047(1975)

[40] V. Chaloupka *et. al.,* Phys. Lett. 61 B, 487(1976).

[41] P. Benkheiri *et. al.,* Phys. Lett. 68 B, 483(1977).

[42] J. Bodenkamp *et. al.,* Phys. Lett. 133 B, 275(1983).

[43] B.G. Gibbard *et. al.,* Phys. Rev. Lett. 42, 1593(1979).

[44] R. Bizzarri *et. al.,* Phys. Rev. D 6, 160(1972).

[45] J. Bensinger *et. al.,* Phys. Rev. D 23, 1417(1983).

[46] J. Z. Bai *et al.* [BES Collaboration], Phys. Rev. Lett. **91**, 022001 (2003) [arXiv:hep-ex/0303006].

[47] M.W. Eaton *et. al.,* Phys. Rev. D 29, 805(1984).

[48] W. Struczinski, et al., *Nucl. Phys.***B108**, 45 (1976).

[49] E.I. Ivanov, *et al.*, *Phys. Rev. Lett.***86**, 3977 (2001).

[50] A. P. Szczepaniak and M. Swat, /it Phys.Lett.**B115**:72-76, (2001).